Supporting Information

Photosensitized membrane permeabilization requires contact-dependent reactions between photosensitizer and lipids

Isabel O. L. Bacellar,[†,‡] Maria Cecilia Oliveira,[§] Lucas S. Dantas,[†] Elierge B. Costa,[§] Helena C. Junqueira,[†] Waleska K. Martins,[‖] Andrés M. Durantini,[‡] Gonzalo Cosa,[‡] Paolo Di Mascio,[†] Mark Wainwright,[⊥] Ronei Miotto,[§] Rodrigo M. Cordeiro,[§] Sayuri Miyamoto,[†] Mauricio S. Baptista[†,*]

[†]Departamento de Bioquímica, Instituto de Química, Universidade de São Paulo, Av. Prof. Lineu Prestes 748, São Paulo, SP, Brazil, 05508-900.

[‡]Department of Chemistry and Center for Self-Assembled Chemical Structures CSACS/CRMAA, McGill University, 801 Sherbrook Street West, Montreal, QC, Canada, H3A 0B8.

[§]Centro de Ciências Naturais e Humanas, Universidade Federal do ABC, Avenida dos Estados 5001, Santo André, SP, Brazil, 09210-580.

[‖]Universidade Anhanguera de São Paulo, Av. Raimundo Pereira de Magalhães, 3305, São Paulo, SP, Brazil, 05145-200.

[⊥]School of Pharmacy & Biomolecular Sciences, Liverpool Jonh Moores University, Liverpool, United Kingdom, L3 3AF

*corresponding author: baptista@iq.usp.br

Contents

1. Materials and Methods

1.1. Materials

Cadmium acetate, 5(6)-carboxyfluorescein (CF), deuterium oxide, diethylenetriaminepentaacetic acid (DTPA), formic acid, glucose, iron(II) chloride tetrahydrate, iron(III) chloride hexahydrate, methylene blue (MB), β-Nicotinamide adenine dinucleotide reduced disodium salt hydrate (NADH), phosphate buffered saline (PBS), potassium iodide, 1-pyrenebutyric hydrazide (PBH), Sephadex G-50, sodium borohydride, sodium dodecyl sulfate (SDS), sucrose, *tert*-butyl hydroperoxide solution (70% in water) and Triton X-100 were acquired from Sigma Aldrich (Saint Louis, MO). 1-Palmitoyl-2-(9'-oxo-nonanoyl)-*sn*-glycero-3-phosphocholine (ALDOPC), 1,2-dimyristoyl-*sn*-glycero-3-phosphocholine (DMPC), 1,2-dioleoyl-*sn*-glycero-3-phosphocholine (DOPC), 1,2-dipalmitoyl-*sn*-glycero-3-phosphocholine (DPPC), 1-palmitoyl-2-arachidonoyl-*sn*-glycero-3-phosphocholine (PAPC), 1-palmitoyl-2-oleoyl-*sn*-glycero-3-phosphocholine (POPC) and 1-palmitoyl-2-(5'-oxo-valeroyl)-*sn*-glycero-3-phosphocholine (POVPC) were acquired from Avanti Polar Lipids (Alabaster, AL). Acetic acid, ascorbic acid, ammonium thiocyanate, hydrochloric acid, iron (III) chloride hexahydrate, perchloric acid, potassium dichromate, potassium dihydrogen phosphate, sodium chloride, sodium molybdate dihydrate, sulfuric acid and tris(hydroxymethyl) aminomethane were bought from Labsynth (Diadema, Brazil). Solvents were acquired from J.T. Baker in HPLC grade. DO15 and H_2B-PMHC were synthesized as previously reported[1,2]. Milli-Q water was used for preparing all aqueous solutions.

1.2. Liposome Membrane Permeabilization

Lipid films containing 15 mg of POPC (or PAPC, for Figure S9 only) were prepared from evaporation of stock solutions in chloroform. The films were hydrated with 0.5 mL of a 50 mM CF solution in 10 mM Tris buffer (pH = 8). Short sonication (30 s) in an ultrasonic bath USC1400-A (Unique – Indaiatuba, Brazil) and vortexing were used to completely detach the lipid film. The resulting suspensions were extruded through a polycarbonate membrane (50-nm pore diameter, Whatman – Maidstone, England) using a mini-extruder from Avanti Polar Lipids. The extruded suspensions were eluted through a Sephadex G-50 column equilibrated with a 0.3 M sodium chloride solution in 10 mM Tris buffer (pH = 8), in order to remove non-encapsulated CF. At this pH CF is anionic and does not cross the membrane; consequently, the resulting liposome suspension only contains CF in the inner compartment of the liposomes. The fact that CF's fluorescence is self-quenched at 50 mM concentration allows monitoring the leakage of this molecule to the outer solution, given that dilution therein will result in fluorescence intensity increase[3–5].

Samples were prepared in a 96-well microplate, with each well containing 15 μL of lipid suspension, 15 μM photosensitizer (MB or DO15, except for controls without photosensitizer) and enough of a 0.3 M sodium chloride solution in 10 mM Tris buffer (pH = 8) to reach a 300-μL volume. CF fluorescence was monitored using a SpectraMax i3 microplate reader (Molecular Devices – Sunnyvale, CA), exciting at 480 nm and detecting at 517 nm. The same equipment was used to measure absorbance of MB (at 633 nm) or DO15 (at 680 nm) under the same conditions. Irradiation was performed with a LED array with maximum emission at 631 nm and FWHM of 18 nm. In the irradiation area and at a 20-cm distance from the light source, the irradiance was of 72 ± 1 W m^{-2}, as determined with a Fieldmate power meter (Coherent - Portland, OR) coupled to a OP2-Vis detector. CF

enhancement values were calculated by dividing the fluorescence intensity at any given time by the initial fluorescence intensity of the same sample.

1.3. Effect of Bleached DO15 on Membrane Permeability

POPC liposomes with entrapped CF were prepared according to item *1.2*, following the same proportions and concentrations of photosensitizer (15 μM) and lipids as described before. However, in this case samples were upscaled to a final volume of 2000 μL and placed in quartz cuvettes, allowing for oxygen removal when necessary. Except for a positive control consisting of liposomes irradiated in the presence of DO15 (30 min, LED array, 631 nm, 72 ± 1 W m^{-2}), all remaining samples contained 0.24 mM NADH (added from a freshly prepared aqueous solution) and were kept in the dark for the whole length of the experiment (30 min). The latter samples consisted of liposomes in the presence of (i) NADH only; (ii) NADH and DO15; (iii) NADH and bleached DO15. Bleached DO15 was obtained by bubbling with argon for *ca.* 15 min a cuvette containing NADH and DO15, irradiating this solution mixture for *ca.* 5 min (LED array, 631 nm, 72 ± 1 W m^{-2}) and only then injecting liposomes into the cuvette through a rubber septum. Fluorescence spectra were recorded with a Cary Eclipse Fluorescence Spectrophotometer (Varian) in the 500-650 nm range (excitation at 480 nm) in three different moments: (i) just after sample preparation; (ii) after 30 min in the dark (samples with NADH) or under irradiation (DO15 only); (iii) once again after the second measurement, but with addition of 0.1% Triton X-100. For each sample, the CF emission intensity at 517 nm obtained after solubilizing the lipids with Triton X-100 (step iii above) was taken as 100%, with the remaining measurements being expressed as percentages of this value.

1.4. Photosensitizer Binding to Liposomes

Membrane binding equilibrium constants of photosensitizers (K_b) were estimated by separating unbound and bound photosensitizers molecules by the use of liposomes that sediment upon centrifugation[6–9]. Two 30 mg POPC films were hydrated with 1 mL water each. The resulting suspensions were centrifuged at 17,000 g for 3 min, after which the supernatants were discarded and the sediments were suspended with 1 mL water. This centrifugation and re-suspension step was repeated two more times, after which both suspensions were united. Eppendorf tubes were then prepared with variable volumes of liposome suspension (0-150 μL) and completed with photosensitizer solutions and water to a final volume of 1.150 mL and 15 μM photosensitizer concentration. Samples containing no liposomes included 150 μL of a surfactant solution consisting of 50 mM SDS + 10% (v/v) Triton X-100 in water. After 30 min of incubation, samples were centrifuged, the supernatants were removed and mixed to equal volumes of surfactant solution, while the sediments were dissolved with 1 mL of surfactant solution. The addition of surfactants prevents photosensitizer aggregation and dissolves liposomes. For each sample, UV-Vis absorption spectra of both fractions were acquired, and the absorbance value at λ_{max} was used to calculate the photosensitizer molar fraction (Y_{PS}) bound to liposomes or dissolved in water. To calculate K_b, the total photosensitizer concentration ($[PS]_T$) was considered to be the sum of the concentrations of photosensitizers bound to lipids or dissolved in water ([PS-L] and [PS], respectively). These concentrations are related by $K_b[L] = [PS\text{-}L]/[PS]$. For the sediment and the supernatant, $Y_{PS} = [PS\text{-}L]/[PS]_T$ and $Y_{PS} = [PS]/[PS]_T$, respectively. Based on the Beer-Lambert law, $[PS]_T$ was considered to be proportional to the absorbance of the sample without liposomes, [PS-L] to half of the absorbance of the

sediment fraction, and [PS] to the absorbance of the supernatant fraction. Y_{PS} was plotted as a function of the lipid concentration ([L]), which was measured[10] as 27.8 mM. For the sediment fraction the model $Y_{PS} = K_b[L]/(K_b[L] + 1)$ was fitted to the graphs, while $Y_{PS} = 1/(K_b[L] + 1)$ was fitted for the supernatant fractions.

1.5. Singlet Oxygen Generation for Photosensitizers in the Presence of Liposomes

POPC liposomes were prepared as in *1.2*, but hydration employed only water. After extrusion, samples with 15 μM photosensitizer, 27 μL of liposome suspension and water to a final volume of 2000 μL were assembled in cuvettes (note that the samples follow the same composition as those that were used for the chemical analysis described in the very next section).

A laboratory version of the TCMPC-1270-LED (SHB Analytics GmbH, Berlin, Germany) was used for direct detection of singlet oxygen phosphorescence kinetics at 1270 nm. The system was used with the extension for custom lasers and rectangular cuvettes. A Quantel Brilliant with Rainbow OPO (Quantel Laser, Les Ulis, France) was used for excitation at 631 nm and 10 Hz. Samples of equal molarity were compared, with 3 independent measurements being performed for 3 independent cuvettes (total of 9 measurements per photosensitizer).

1.6. Preparation of Lipid Samples for Chemical Analysis

The procedure for preparation of POPC films and hydration was the same as for section *1.2*, but hydration employed only water. After extrusion, the suspension was distributed in microplate wells, with all experiments being performed in water and the concentration of photosensitizer being kept at 15 μM. For the quantification of POPC hydroperoxides,

alcohols and ketones (see *1.8*) and for the quantification of aldehydes at similar permeabilization levels (see *1.11*), the liposome suspension volume per well was 4 μL (to correct for the higher lipid concentration if compared to the CF-containing suspensions, which are diluted in the exclusion chromatography step). For the quantification of POPC-derived aldehydes described in *1.10*, the liposome suspension volume was raised to 10 μL, to ensure aldehyde detection even if at low levels. The same irradiation procedure from section *1.2* was employed, with samples being collected from wells at different irradiation times and immediately transferred to dry ice.

Lipids were then extracted using the Bligh-Dyer method[11]. Different experiments used different volumes for extractions, while keeping the same proportions between solvents. Briefly, the sample (0.8 volume), methanol (2 volumes) and chloroform (1 volume) were added to a tube, in addition to a small volume of an internal standard solution. After the mixture being vortexed and a homogeneous mixture being obtained, chloroform (1 volume) and water (1 volume) were added to the tube, which was centrifuged at 1,500 g for 2 min. The lower phase was collected and a re-extraction was carried out by addition of extra chloroform to the tubes. The combined collected fractions were dried under a nitrogen flux. For the quantification of POPC hydroperoxides, alcohols and ketones (see *1.8*), the sample volume was 280 μL, the extract was dissolved in 875 μL of methanol and the final concentration of internal standard (DPPC) was 10 μg mL^{-1}. For the quantification of POPC-derived aldehydes (see *1.10*), the sample volume was 1120 μL, the extract was dissolved in 80 μL of isopropyl alcohol and the final concentration of internal standard (POVPC) was 8 μg mL^{-1}. For the quantification of aldehydes at similar permeabilization levels (see *1.11*), the sample volume was 250 μL, the extract was dissolved in 35.7 μL of isopropyl alcohol and the final concentration of internal standard (POVPC) was 8 μg mL^{-1}.

1.7. UHPLC-UV Analysis of POPC Oxidation Products

Ultra-high performance liquid chromatography with ultraviolet absorption detection (UHPLC-UV) was employed to analyze POPC oxidation products. Analyses were carried out in a Shimadzu UHPLC Nexera chromatograph equipped with a SPD-M20A PDA detector, operating from 190 to 300 nm. A C8 Kinetex column (100 x 2.1 mm, 1.7 μm, Phenomenex) was employed and samples were eluted at 40 ^{o}C with a water/acetonitrile linear gradient at 0.5 mL min^{-1} flow rate. The percentage of acetonitrile was kept at 63% for the initial 17 min, raising to 100% at 18 min and keeping at this percentage until 23 min, when it started decreasing. At 25 min acetonitrile percentage was back to 63%, and held at this level until the end of the run at 30 min. The injection volume was 5 μL, employing already extracted samples.

1.8. Quantification of POPC Hydroperoxides, Alcohols and Ketones

Chromatographic separation employed a Shimadzu HPLC system equipped with a SCL-10A VP controller and the software CLASS-VP. A Luna C8 column (250 x 4.6 mm, 5 μm, Phenomenex) was used at room temperature. The eluent was a mixture with 3% water (v/v), 97% methanol (v/v) and 0.1 % formic acid (v/v). The flow rate was kept at 1 mL min^{-1}, being a splitter used to direct *ca.* 12% of it to the mass spectrometer. For POPC and for hydroperoxides quantification, the injection volume was 10 μL of the lipid extract (see *1.6*). For alcohols and ketones, the injection volume was raised to 50 μL of the same extracts. A Quattro II (Micromass, Manchester, UK) mass spectrometer controlled by the software MassLinx 3.2 was employed for the analyses. Detection was achieved by electrospray ionization (ESI) in the positive mode, with the following conditions: source temperature:

150 ^{o}C; desolvation temperature: 200 ^{o}C; sample cone voltage: 30 V; capillary voltage: 4500 V; extraction cone voltage: 10 V; collision energy: 30 eV; drying gas: nitrogen at 400 L h^{-1}; nebulizing gas: nitrogen at 30 L h^{-1}; collision gas: Ar. Initially, full scan spectra (100-1000 *m/z*) from the samples and synthesized lipids were acquired, in addition to product ion (PI) scans of the ions $[M+H]^+$ and $[M+Na]^+$. The transition $[M+H]^+ \rightarrow$ *m/z* 184.1, corresponding to the loss of phosphocholine[12] and being the most intense one, was chosen to quantify the lipids by multiple reaction monitoring (MRM). The peak areas of the studied transitions (POPC: *m/z* 760.6 → 184.1; POPC hydroperoxides: *m/z* 792.6 → 184.1; POPC alcohols: *m/z* 776.6 → 184.1; POPC ketones: *m/z* 774.6 → 184.1) were normalized by that of the internal standard (DPPC: *m/z* 734.6 → 184.1). Calibration curves were constructed with the synthesized oxidized lipids (see *1.12*, *1.13*, *1.14*) and POPC, employing DPPC as an internal standard in all cases. We observed the presence of smaller quantities of Na^+ adducts, but the proportion to H^+ adducts was constant in all samples, making corrections unneeded. Moreover, the transition $[M+Na]^+ \rightarrow [M+Na-59]^+$ (loss of trimethylamine[13]) produces lipid-specific fragments, which were additionally used to confirm the identity of the of the analytes (POPC: *m/z* 782.6 → 723.5; POPC hydroperoxides: *m/z* 814.6 → 755.5; POPC alcohols: *m/z* 798.6 → 739.5; POPC ketones: *m/z* 796.5 → 737.5; DPPC: *m/z* 756.6 → 797.5).

1.9. Derivatization of Lipid Aldehydes

For the samples employed for POPC-derived aldehydes quantification, extraction (see *1.6*) was followed by derivatization with the aldehyde-specific probe PBH[14]. For the quantification of POPC-derived aldehydes (see *1.10*), the lipid extract in isopropyl alcohol (80 μL) was mixed with 12.5 μL of a 4 mM PBH solution and 10 μL of 10 mM formic

acid. For the detection of aldehydes at similar permeabilization levels (see *1.11*), the lipid extract in isopropyl alcohol (35.7 μL) was mixed with 5.58 μL of a 4 mM PBH solution and 4.46 μL of 10 mM formic acid. The mixtures were then kept under agitation at 37 ^{o}C for 6 h before analysis. As a control, POPC hydroperoxides were treated with PBH and no PBH adducts were detected.

1.10. Quantification of POPC-Derived Aldehydes

Lipid extracts derivatized with PBH (see *1.6* and *1.9*) were analyzed by ESI-TOFMS (time of flight MS, Triple TOF 6600, Sciex, Concord, US) interfaced with a Nexera UHPLC system. The injection volume was set at 15 μL, and the first minute of run was not sent to the mass spectrometer, to discard the highly-concentrated PBH. Samples were eluted through a Kinetex C18 column (50 x 3.0 mm, 2.6 μm, Phenomex) with a water/methanol linear gradient (0.1% formic acid), with 0.6 mL min^{-1} flow rate and at 40 ^{o}C. During the first 7 min of run, the methanol percentage linearly increased from 88% to 95%. The methanol percentage was held at 95% from 7-10 min and decreased to 88% from 14-15 min, staying at this value until the end of the run, at 18 min. The mass spectrometer was operated in positive ionization mode, and the scan range was set at *m/z* 200-2000. Data for lipid identification and quantification was obtained by PI of each specific mass. Data acquisition was performed with a period cycle time of 275 ms with 100 ms acquisition time for MS1 scan and 25 ms acquisition time for MS2. Data acquisition was performed using Analyst 1.7.1 with 5.5 kV ion spray voltage and 80 V cone voltage. The curtain gas was set at 30 psi, nebulizer and heater gases at 50 psi, and the interface heater at 600°C. The MS/MS data was analyzed with PeakView (Sciex) and lipid quantification was performed with MultiQuant (Sciex) softwares, where peak areas of the mass transitions (ALDOPC-8-

PBH: *m/z* 920.55 → 184.07; ALDOPC-PBH: *m/z* 934.57 → 184.07; ALDOPC-10-PBH: *m/z* 946.57 → 184.07) were normalized by that of the internal standard (POVPC-PBH: *m/z* 878.51 → 184.07). The *m/z* 271.11 fragment, corresponding to the pyrene butyric group, was used for identity confirmation. Data were compared with a calibration curve obtained with commercial ALDOPC and using POVPC also as internal standard (being both lipids also derivatized with PBH). Since ALDOPC-8 and ALDOPC-10 are expected to ionize similarly to ALDOPC, but are not commercially available, all lipids were quantified using the same calibration curve.

1.11. Relative Quantification of POPC-derived Aldehydes at Similar Permeabilization Levels

The same chromatographic and MS conditions from *1.10* were employed for the quantification at lipid aldehydes at similar permeabilization levels, with lipid extracts being prepared according to *1.6* and *1.9*. The different irradiation times for MB and DO15 were set so that similar CF enhancement levels (see *1.2*) were reached.

1.12. Synthesis of POPC Hydroperoxides

POPC hydroperoxides were synthesized by singlet oxygen oxidation of POPC, using MB as a photosensitizer[15,16]. 50 mg of POPC, 250 µL of a 10 mM MB solution in methanol and 20 mL of chloroform were added to a round-bottom flask. For 2.5 h, the mixture was kept under agitation in an ice bath and under oxygen atmosphere, while being irradiated with a 500 W tungsten lamp. The reaction was followed by UHPLC-UV, using the method from section *1.7*. The mixture was then rotaevaporated, dissolved in a smaller volume of methanol and eluted through a silica column equilibrated with a chloroform/methanol 1:1,

in order to remove MB. The product was purified by HPLC at room temperature, using a semi-preparative Luna C18 column (250 x 10 mm, 5 μm, Phenomenex – Torrance, CA) and methanol (5 mL min^{-1}) as an eluent. The collected fractions were united and concentrated in 1 mL of methanol. The product was analyzed by HPLC-MS (see *1.8*) and quantified (see *1.15*), resulting in 24% yield and 28 ± 3 mg mL^{-1} concentration by the iron thiocyanate method (for comparison, concentrations of 27 ± 2 mg mL^{-1} and 22 ± 6 mg mL^{-1} were obtained with iodometry and the molybdate method, respectively).

1.13. Synthesis of POPC Alcohols

The methodology employed to synthesize POPC alcohols was based on reduction of POPC hydroperoxides[15,17,18]. 250 μL of POPC hydroperoxide (see *1.12*), 750 μL of methanol and 1 mg of sodium borohydride were mixed in a test tube in ice. After a 2 h reaction time, 1 mL of water, 20 μL of 10 M hydrochloric acid and 2 mL of a 1:1 hexane/diethyl ether mixture were added to the tube. After the mixture was vortexed and then centrifuged (1,500 g for 1 min), its upper phase was collected. A first re-extraction was carried out with extra 2 mL of the hexane/diethyl ether mixture, and a second one was performed by adding 2 mL of chloroform and collecting the lower phase. The collected fractions were united and concentrated in 0.5 mL of methanol. The product was analyzed by HPLC-MS (see *1.8*) and quantified (see *1.15*), resulting in 68% yield and 9.4 ± 0.5 mg mL^{-1} concentration.

1.14. Synthesis of POPC Ketones

POPC ketones were obtained by oxidizing POPC alcohols with chromic acid[19]. 10 μL of POPC alcohols (see *1.13*) were dried in a test tube using a nitrogen flux. The residue was dissolved with 380 μL of acetone and 20 μL of a chromic acid solution (prepared by mixing

equal volumes of 0.5 M potassium dichromate and 4 M sulfuric acid). The reaction was kept at room temperature for 20 min, being frequently vortexed. Subsequently, 600 μL of water and 1 mL of hexane were added to the tube. After centrifugation, the upper phase was collected and re-extraction was performed with another 1 mL of hexane. The residue of the evaporation of the combined collected phases was dissolved in methanol and purified by HPLC, with the same conditions as for hydroperoxides. A second synthesis was performed with all volumes 7 times larger. The products from both syntheses were united and concentrated in 1 mL of methanol. The combined product was analyzed by HPLC-MS (see *1.8*) and quantified (see *1.15*), resulting in 20% total yield and 0.15 ± 0.01 mg mL^{-1} concentration.

1.15. Quantification of the Synthesized Oxidized Lipids

The synthesized oxidized lipids were quantified by three different methodologies. All the synthesized lipids were quantified by the iron thiocyanate assay, following the procedure described by Stewart[10], comparing the samples to a calibration curve build from a stock solution of POPC in chloroform. Hydroperoxides were also quantified by adapting the method described by Harris[20]. In this case, sample digestion was carried out by adding 10 μL of samples to test tubes containing 0.3 mL of 70% perchloric acid, and heating to 180 ^{o}C for 20 min. Subsequently, 9.3 mL of water, 0.5 mL of a solution a 25 g L^{-1} of sodium molybdate with 2.5% sulfuric acid and 0.5 mL of a 3% ascorbic acid solution were added to the tubes. After heating in a boiling bath for 10 min, absorbances at 830 nm were recorded. These data were compared to a calibration curve, for which variable volumes of a potassium dihydrogen phosphate solution and enough water to complete 9.3 mL were added to the tubes. Hydroperoxides were additionally detected adapting the method

described by Buege & Aust[21]. Initially, samples were diluted 50 times in methanol. 50 μL of the diluted samples, 500 μL of a 3:2 acetic acid/chloroform mixture and 50 μL of a 1.2 g mL^{-1} potassium iodide solution were added to a vial (both solutions were bubbled with nitrogen for 15 min in ice bath prior usage). The mixtures were purged with nitrogen for 5 s, vortexed and kept in the dark for 5 s. Subsequently, 1.5 mL of a 0.5% cadmium acetate solution were added to the flasks and the absorbance of the organic phase was measured at 353 nm. The measurements were compared to the results of a calibration curve, in which the sample was substituted by solutions of *tert*-butyl hydroperoxide in methanol with variable concentrations.

The results obtained by iron thiocyanate assay were employed for future calculations, whereas the remaining assays provided confirmatory and supporting data for hydroperoxides.

1.16. Photobleaching

Samples containing 15 μM photosensitizer in water were placed in a quartz cuvette (1.0 cm x 1.0 cm) with a magnetic stirrer. A diode laser emitting at 650 nm (Laserline – Amparo, Brazil) was employed for irradiation. Light reached the cuvette via an optical fiber, at the extremity of which the light power was 35 mW. UV-Vis absorption spectra (200-800 nm) were acquired with a Shimadzu UV-1800 (Kyoto, Japan) spectrophotometer. For samples containing liposomes, the final lipid (DOPC, DPPC, POPC or POPC hydroperoxides) concentration in the cuvette was 0.5 mM. Liposomes were prepared from a 7.5 mg lipid film, which was hydrated with 1 mL water. The resulting suspension was extruded through a 50-nm pore diameter membrane. Photobleaching rate constants were calculated from the initial instants of plots of absorbance at the main absorption wavelength as a function of

irradiation time, after converting the *y*-axis scale to the natural logarithm of the ratio between the absorbance at a given time and the initial absorbance.

Solely for the experiments aiming to test the effect of the double bond concentration on DO15 photobleaching rates, 44 mM liposome stock solutions were prepared and extruded through a 50-nm pore diameter membrane. Liposomes compositions (mol/mol) were: (i) DMPC; (ii) DMPC:POPC 9:1; (iii) DMPC:POPC 8:2; (iv) DMPC:DOPC 9:1. We note that the choice for DMPC, as opposed to DPPC in the previously reported experiments, was to avoid lipid phase separation at room temperature for the two-components membranes[22]. For each liposome compositions, 8 wells were prepared on a 96-well plate, with 4 μL of liposome suspension, 15 μM DO15 and enough milliQ water to reach a final volume of 300 μL. Samples were irradiated with a LED array (631 nm, 72 ± 1 W m^{-2}) for 10 min, with the absorbance at 680 nm being recorded every 1 min with a SpectraMax i3 microplate reader. Photobleaching rate constants were calculated from plots of absorbance as a function of irradiation time, after converting the *y*-axis scale to the natural logarithm of the ratio between the absorbance at a given time and the initial absorbance.

1.17. H_2B-PMHC Activation by DO15

13.5 nmol of H_2B-PMHC dissolved in acetonitrile were transferred to a glass vial. After removal of the solvent under vacuum, 10 μmol of POPC dissolved in chloroform were added to the flask and a lipid film was obtained by evaporating the solvent under vacuum for 1 h. The resulting film was hydrated with 509 μL of PBS buffer (for experiments carried out in deuterium oxide, a 10x PBS was first evaporated under vacuum and then re-dissolved in deuterium oxide). The resulting liposome suspension was subjected to three

freeze-thaw-sonication cycles, followed by extrusion through a 100-nm polycarbonate membrane. The prepared samples contained 100 μL of H_2B-PMHC-containg liposomes suspension, 0.24 μM DO15 and enough buffer to complete a volume of 2000 μL (*i.e.* leading to 1 mM of POPC and 1.33 μM of H_2B-PMHC). Samples were irradiated with a LED setup (Luzchem) operating at 634 nm, with FWHM of 17 nm and 18.5 W m^{-2} irradiance. Emission scans were recorded as a function of irradiation time, using a PT1 QM4 fluorimeter (excitation: 480 nm; emission: 490-800 nm) and 1.0 cm x 1.0 cm cuvettes. Blank curves obtained with PBS and POPC liposomes were subtracted from corrected emission spectra, and the resulting intensities at the maximum emission wavelength were plotted as a function of irradiation time. Emission enhancement values were calculated by dividing each data point by the initial intensity of the same sample. To calculate enhancement rate constants, linear equations were fitted to data points up to 2 min of irradiation.

1.18. Sensitivity of Giant Unilamellar Vesicles to pH

Giant unilamellar vesicles (GUVs) were prepared by the electroformation method[23], following the procedure described by Mertins *et al.*[8] with minor adaptations. Giant unilamellar vesicles (GUVs) were prepared by the electroformation method23, following the procedure described by Mertins et al.8 with minor adaptations. Lipid films were obtained from 10 μL of 2.0-2.5 mM chloroform solutions of POPC, POPC hydroperoxides, PAPC or PAPC:PAPC hydroperoxides 1:1 (mol/mol, synthesized by us). For hydration of the lipid films, a 0.1 M sucrose solution was employed, with a measured pH of 6.1-6.6. The obtained GUV suspensions were diluted 7-fold in 0.1 M glucose solutions of different pH values in the 2.6-8.1 range (pH previously adjusted by addition of HCl or NaOH). For the

experiments carried out in the presence of Fe(III) or Fe(II) cations, small volumes (<0.2% of the final volume) of the respective chloride salts were added to the sample at the onset of the observation time, resulting in 31 μM concentration of iron cations. The GUVs were then observed in phase-contrast mode in an Axiovert 200 (Carl Zeiss, Germany) inverted microscope with an A-plan 10X/NA 0.25 Ph1 objective (Carl Zeiss) and an AxioCam HSm camera (Carl Zeiss), using the Axivision package for image acquisition.

1.19. Statistical Analyses

Statistical analyses were performed using IBM SPPC Statistics version 20. Data obtained from at least three independent measurements (n = 3) were expressed as mean ± standard error, unless otherwise noted. To perform comparative statistical analysis, we first analyzed the variance between groups. Next, multiple comparisons were carried out using one-way analysis of variance (ANOVA) with Dunnett's T3 or Bonferroni post-hoc test, depending on homogeneity of variance. For comparison between two groups, before comparative analysis we applied the Kolmogorov Smirnov test to evaluate the gaussian adherence of data. To perform parametric and non-parametric tests, we used t-student and Mann-Whitney, respectively. An $\alpha = 5\%$ (p-value < 0.05) was considered to be statistically significant.

1.20. Molecular Dynamics Simulations: Photosensitizer Binding to Membranes

Molecular dynamics simulations were performed using the GROMACS 4.5.1 simulation package[24,25]. Molecular motions were computed by numerical integration of Newton's equations with a time step of 2 fs. Fully hydrated lipid bilayers made of POPC were represented using the force field developed by Kukol[26]. The interaction parameters were

based on the GROMOS53A6 force field[27], in which aliphatic carbon atoms and their adjacent hydrogens are treated as united atoms. To simulate fully hydrated lipid bilayers, the SPC model[28] was used for water. A sole oxygen molecule was added to the aqueous phase. The oxygen molecule dissolved in the membrane was described with parameters taken from the literature[29]. For compatibility, MB and DO15 were assembled using the standard functional groups in the GROMOS53A6 force field[27]. The partial charges of MB and DO15 were taken from density functional calculations performed using the Gaussian package[30].

Starting configurations for molecular dynamics were obtained from a pre-equilibrated membrane patch with 128 lipid molecules. The photosensitizers were initially placed at the aqueous phase at a distance of *ca.* 3 nm from the bilayer surface. Sets of eight MB or DO15 molecules were added. Cl^- ions were added to neutralize the system. Overall, each simulated system had lateral dimensions of *ca.* 6.2 nm parallel to the membrane surface (*xy* plane) and *ca.* 8.5 nm along the bilayer normal (*z* axis). Periodic boundary conditions were applied in all Cartesian directions. The simulation protocol started with an equilibration run for 5.5 ns, during which the position of the photosensitizers was kept restrained. The molecules were then released and molecular trajectories were recorded for 500 ns under controlled temperature (310 K) and pressure (1 atm).

Photosensitizer binding to membrane was followed in time by recording both the position and the orientation of the different photosensitizers with respect to the bilayer. Density distributions of the membrane building blocks, oxygen and the photosensitizer were calculated along the *z* axis. The density distribution overlaps were obtained following the scheme described in [31]. All density distribution profiles were normalized in order to allow

the comparison between DO15 and MB results. Further details of our theoretical modeling can be found in [31].

1.21. Molecular Dynamics Simulations: Oxidized Membranes

Molecular dynamics simulations were performed using the GROMACS 5.0.4 package[24,25]. Newton's equations of motion were numerically solved with a 2 fs time step. Interatomic interactions, temperature and pressure were treated as in previous simulations of oxidized membranes[32]. Well validated models were used for the description of unsaturated lipids[33] and lipid hydroperoxides[32]. These models were expanded to include a larger variety of lipid oxidation products, as shown in Figure S1. Interatomic interaction parameters for the alcohol, aldehyde and ketone functional groups were taken from the standard GROMOS 53A6 force field library[27,34]. The internal rotation of the enone moiety was described according to spectroscopic data[35]. The effect of *cis* to *trans* isomerization at the acyl chain unsaturation was incorporated in the structure of lipid oxidation products[36]. In cases where the oxidized functional groups were stereogenic, we considered only the R stereoisomer for simplicity. Fully hydrated bilayers were assembled with 64 lipids per leaflet. Each bilayer contained only one type of lipid: either the pristine POPC, or one of its oxidation products. Membranes were equilibrated for at least 300 ns under controlled temperature (310 K) and pressure (1 atm). As depicted in Figure S15, well-converged membrane properties were obtained. The last 100 ns of simulation trajectories were used for the calculation of average properties such as the area per lipid and the membrane thickness.

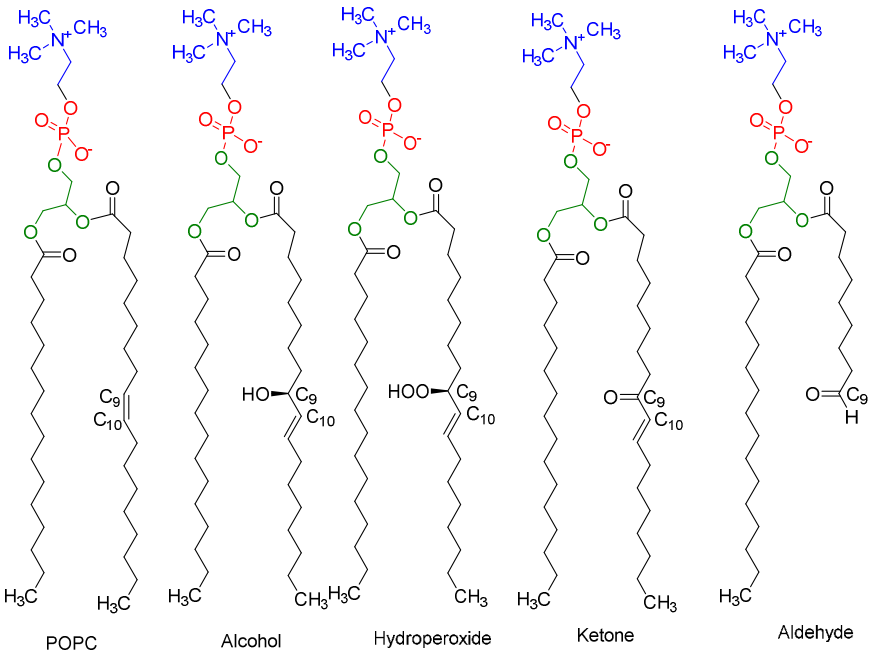

Figure S1. Structures of POPC and of lipid oxidation products, representing the specific isomers employed for molecular dynamics simulations.

We also monitored the location of the functional groups and membrane hydration. Very few water molecules managed to populate the membrane interior. However, the number increased for oxidized membranes. The free energy profile for water permeation was derived from the distribution of water molecules across the membrane, according to:

$$\Delta G(z) = -k_B T \ln \frac{\rho(z)}{\rho_\infty} \tag{S1}$$

where k_B is the Boltzmann constant, T the temperature, $\rho(z)$ the distance-dependent number density of water molecules and ρ_∞ its bulk value.

2. Additional Figures, Tables and Calculations

2.1. Experimental Studies of the Interaction of MB and DO15 with POPC Bilayers

As discussed in a previous publication[7], spectral changes can be taken as evidence for interactions between photosensitizers and lipid bilayers. Namely, interaction with membranes shifts aggregation equilibria of amphiphilic phenothiazinium photosensitizers (*e.g.*, DO15) towards monomerization, increasing the monomer's absorption band. For hydrophilic photosensitizers (*e.g.*, MB), however, none or only subtle changes were reported. The same effect was presently observed in the studied membrane model (Figure S2A-B), employing different lipid compositions. For MB, addition of either POPC or POPC hydroperoxide liposomes did not lead to significant changes if compared to water. On the other hand, addition of liposomes to a DO15 aqueous solution increased its absorbance, suggesting that DO15 interacts with liposomes. Following the absorption increase trend, we infer that this interaction is less extensive with DPPC liposomes, but very similar for DOPC, POPC or POPC hydroperoxides. The smaller interaction with DPPC is probably a consequence of DPPC membranes being in the gel phase at room temperature[37].

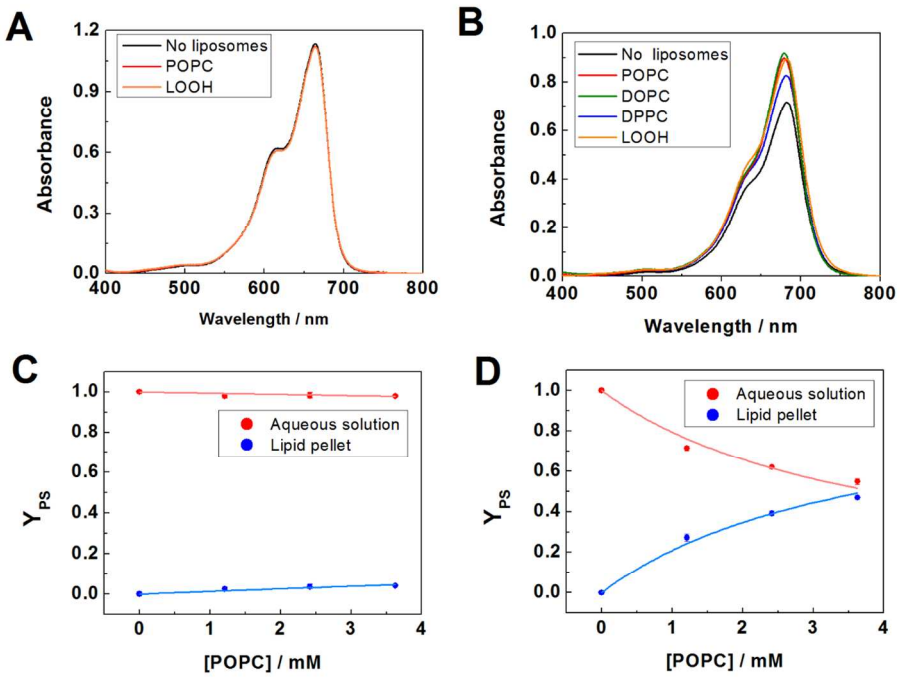

Figure S2. Absorption spectra of (A) MB and (B) DO15 in the water or in the presence of liposomes with different composition of lipids (POPC, DOPC, DPPC or POPC hydroperoxides, LOOH). For samples containing liposomes, spectra were corrected for scattering. Graphs (C) and (D) are membrane binding isotherms for POPC liposomes, constructed by incubation of liposomes with a photosensitizer solution, followed by separation of the aqueous and membrane fractions by centrifugation. See *1.4* for a description of the model fitted to the curves (full lines).

The supposition that MB interacts less with membranes than DO15 was confirmed by measuring the equilibrium binding constant (K_b) for POPC liposomes (Figure S2C-D and Table S1). K_b was determined in two different ways, which yielded similar results (*i.e.* by measuring photosensitizer concentrations in the lipid fraction or in the aqueous fraction of liposomes suspensions after centrifugation at 17,000 g – see methods section 1.4). Taking the values determined in lipid fractions (where photosensitizer concentration is lower and small variations are more significant), we conclude that, under the lipid concentrations used for CF leakage assays and for chemical analysis of lipid photooxidation products, there are *ca.* 7 times more DO15 molecules dissolved in water than in membranes, while for MB the number rises to *ca.* 150 times more photosensitizer molecules in the aqueous medium.

Table S1. Binding constants (K_b) for MB and DO15 in POPC liposomes, as determined by incubation of liposomes with a photosensitizer solution, followed by separation of the aqueous and membrane fractions by centrifugation. Values resulting from both fractions are displayed below, in addition to the R^2 value of the fit to isotherms of Figure S2C-D.

	K_b / M^{-1} [R^2]	
	Lipid pellet	**Aqueous solution**
MB	13 ± 2	6.1 ± 0.9
	[0.84]	[0.92]
DO15	(2.7 ± 0.1) x 10^2	(2.6 ± 0.2) x 10^2
	[0.99]	[0.99]

2.2. Computational Studies of the Interaction of MB and DO15 with POPC Bilayers

Molecular dynamics simulations were carried out in order to understand the molecular details of the interaction of MB and DO15 with POPC bilayers. Figure S3 shows density profiles along the *z* axis (normal to the bilayer) for MB and DO15, as well as for oxygen, POPC's phosphate groups and carbon chain unsaturation. When penetrating in the membrane, the photosensitizers distributed mostly between the phosphate group and the carbon chain unsaturation. It is noticeable that DO15 density profile resulted from two populations, differently from MB. Besides taking longer to penetrate into the bilayer, DO15 also visited the more polar regions more often than MB (Figure S4), leading to the density distribution component shallower in the membrane. Still, DO15 density distribution overlapped more both with the carbon chain unsaturation (30 %) and with oxygen (5 %) if compared with MB (Table S2). Expectedly, its overlap with the phosphate group was lower than for MB, being 80% of it. The reader is referred to [31] for further details about calculations of the overlap.

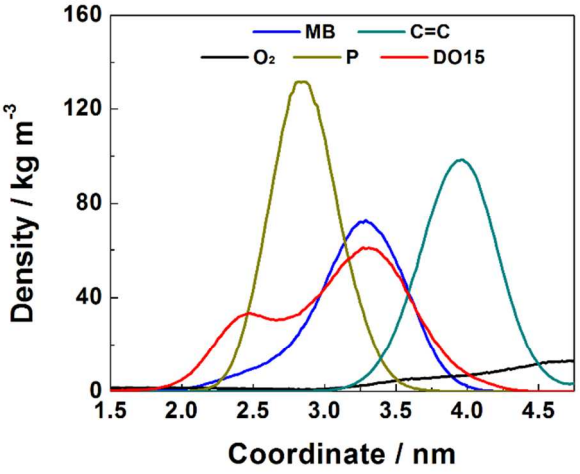

Figure S3. Density profiles along a segment of the z axis (full dimension: 8.5 nm) for the photosensitizers MB and DO15, as well as for oxygen (O_2), POPC phosphate groups (P) and POPC carbon chain unsaturation (C=C). The graph shows only half of the bilayer, with the other half being symmetrical.

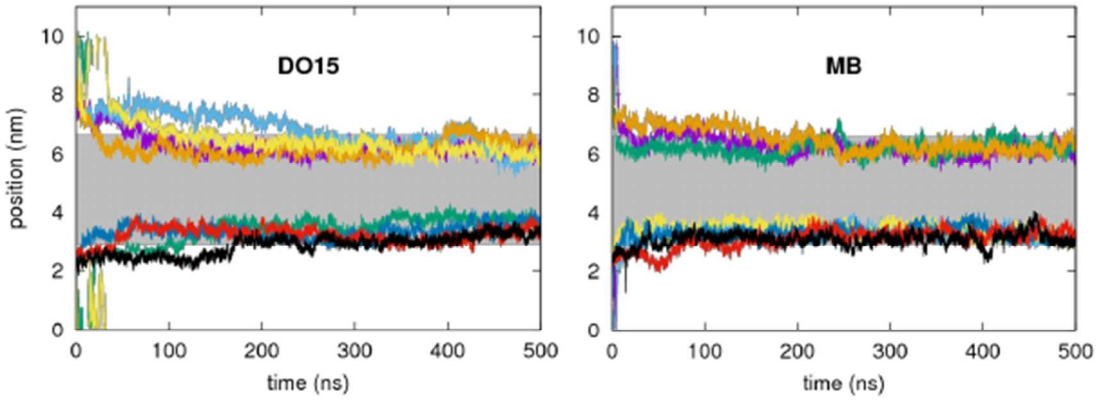

Figure S4. Immersion depth as a function of time for molecular dynamics simulations of DO15 and MB in POPC bilayers. The shaded area corresponds to the membrane interior.

Table S2. The first two columns show the overlap (arbitrary units) of the density profiles shown in Figure S3 for oxygen (O_2), POPC phosphate groups (P) and POPC carbon chain unsaturation (C=C) with the distribution profiles of MB and DO15. The third column shows the ratio between the calculated overlaps for DO15 and MB.

	MB	DO15	DO15 / MB
O_2	12965	13672	1.05

P	236980	189272	0.80
C=C	68935	89870	1.30

2.3. Estimation of Photosensitizer Efficiencies for Contact-Independent and Contact-Dependent Processes

Experimental and computational data on the interaction of MB and DO15 with POPC bilayers allowed us to calculate the efficiency of these photosensitizers to both *(i)* generate singlet oxygen molecules that can reach the bilayer, consequently allowing us to estimate the efficiency of the ene reaction for each photosensitizer (*i.e.* efficiency of contact independent processes); and to *(ii)* establish molecular contact with the lipid double bond to initiate contact-dependent reactions with lipids. Our calculations focus on the initial stages of photosensitization reactions, hence disregarding consumption of reactants and photobleaching. Below, we first develop our model for contact-independent processes and the follow for contact-dependent ones.

The number of singlet oxygen molecules generated by a photosensitizer per unit time (Q) can be calculated by

$$Q_{\Delta} = \Phi_{\Delta} \lambda_i P_i \sigma_i (hc)^{-1} \quad \text{(S2)}$$

where λ_i is the irradiation wavelength, P_i is the irradiance of the light source, σ is the absorption cross-section of the photosensitizer (see [38]) at the irradiation wavelength, and hc is the product of Planck's constant and the speed of light[39]. The parameters from Table S3 lead to Q_{Δ} values of 2.53 and 1.36 singlet oxygen molecules s^{-1} for MB and DO15, respectively, which would actually predict inverted photosensitizer efficiencies if compared to our experimental results (*e.g.*, membrane permeabilization and lipid oxidation efficiencies).

Table S3. Irradiation wavelength (λ_i), irradiance of the light source (P_i), absorption cross-section of the photosensitizer at λ_i (σ) and singlet oxygen quantum yield (Φ_Δ)[7] for MB and DO15.

	MB	**DO15**
λ_i / nm		631
P_i / W m^{-2}		72
σ / Å^2	2.13	1.21
Φ_Δ	0.52	0.49 ± 0.02

However, in microheteregenous systems singlet oxygen production is not spatially homogeneous. In order to account for this effect, we need to consider the geometry of the liposomes in suspension, since the number of singlet oxygen reaching each liposome's membrane depends on the number of membrane-embedded photosensitizers per liposomes and also on the number of photosensitizer molecules that are close enough to the membrane to still allow singlet oxygen molecules to reach the membrane under an average lifetime. Both numbers depend on the partition of the photosensitizer between water and membrane and on the concentrations of liposomes and photosensitizers, as exemplified in Figure S5. POPC liposomes with 50 nm diameter have *ca.* 1.9 x 10^4 lipid molecules, as calculated from the ratio of the total area of a spherical shell with the thickness of a POPC membrane and the area occupied per lipid. Therefore, in a 0.53 mM POPC solution, which was the final concentration in the studied samples (as determined by HPLC-MS, see *1.8*), the liposome concentration was 28 nM. Considering that the average diffusion distance of a singlet oxygen molecule in water is *ca.* 86 nm (calculated as $(D_\Delta \tau_\Delta)^{1/2}$, with D_Δ being the diffusion coefficient of singlet oxygen in water, 2 x 10^{-5} cm^2 s^{-1}, and τ_Δ being the singlet

oxygen lifetime in water, 3.7 μs)[40], one can extend the radius of each liposome by this distance to account for singlet oxygen molecules that will be generated in water and can still reach the membrane. The volume corresponding to the liposome radius extended by 86 nm will be then referred as "active singlet oxygen volume". It is important to emphasize that the active singlet oxygen volume and the employed liposome concentration are sufficiently small in order to assume that most of the times the species generated close to one liposome will not reach other liposomes.

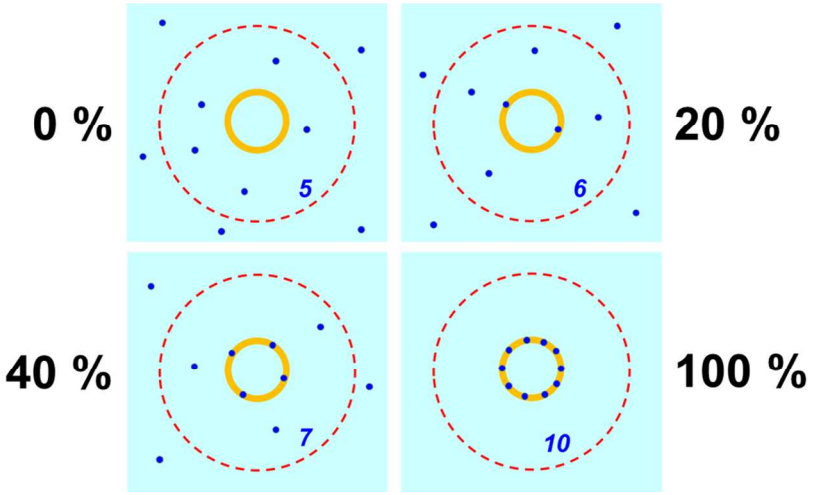

Figure S5. The percent incorporation of photosensitizers into membranes can affect the number of singlet oxygen molecules reaching the bilayer. In the selected example, when all photosensitizer molecules are dissolved in water, only 5 generate singlet oxygen under the average diffusion distance of singlet oxygen, indicated by the red circle. When all the molecules are in the membrane, the number grows to 10. Intermediate binding percentages lead to intermediated quantities of photosensitizers generating singlet oxygen molecule that in average can reach the membrane.

For a 15 μM photosensitizer solution, in the extreme case where all photosensitizers are incorporated in the membrane, there would be 542 photosensitizers per liposome and none in the surrounding solution. In the opposite scenario, where all photosensitizers are solubilized in water, there would be no photosensitizer in the membrane, but still 52

photosensitizers in the active singlet oxygen volume. MB and DO15 fall in intermediate cases: for DO15 there are 76 photosensitizers in the membrane and extra 44 dissolved in water in the active singlet oxygen volume; for MB, there are only 4 in the membrane and 51 in the surrounding aqueous solution. When each of these numbers is multiplied by the number of singlet oxygen molecules generated per second (Q) and summed, DO15 generates 163 molecules per second that would be able to reach the membrane, while MB generates140. We note that 1 in every 5 singlet oxygen molecules are expected to react with the double bonds, as calculated by Weber *et al.*[41]. Broadly speaking, singlet oxygen molecules that are generated within the membrane have the same fate of any other singlet oxygen molecule generated in the vicinity solution, which is to diffuse. In terms of targeting membranes, this basically means that the vast majority of the singlet oxygen molecules that are generated within the membrane will simply diffuse out of the membrane, as much as those generated within the diffusion pathway close the membranes will diffuse into the membrane. In other words, unless there are very reactive compounds included in the membrane, the chance that a membrane-generated singlet oxygen molecule reacts within the membrane is the same as for a singlet oxygen molecule generated within the diffusion pathway. Indeed, when one measures the singlet oxygen kinetics for membrane embedded photosensitizers, the main contribution to the signal comes from molecules escaping the membrane[42].

In order to assess the frequency of encounters of triplet states of the photosensitizer with double bonds, we first estimate the number of triplet excited states generated by a photosensitizer per unit time (Q_T):

$$Q_T = \Phi_T \lambda_i P_i \sigma_i (hc)^{-1} \quad \text{(S3)}$$

where Φ_T is the triplet-excited state generation quantum yield. For phenothiazinium photosensitizers in oxygenated solutions, $\Phi_T \sim \Phi_\Delta$ [43], meaning that Q_T can be well approximated by the previously calculated value of Q_Δ. Hence, 2.53 and 1.36 photosensitizer triplet excited states are generated per second per molecule of MB and DO15, respectively. While the diffusion coefficient of photosensitizers in water (D_{PS}) has been extensively characterized for MB and the best estimate is 4.6 x 10^{-6} cm^2 s^{-1} (see [44]), for DO15 we estimated D_{PS} to be 4.3 x10^{-6} cm^2 s^{-1}, considering the variation of diffusion coefficient for other dyes as a function of molecular weight[45,46].

In aqueous solution, MB has a triplet excited state lifetime (τ_T) of *ca.* 1.5 μs [47], which is similar to that of DO15, as both dyes display very similar photophysics[7,47]. Therefore, both molecules are expected to have similar average diffusion distances of $(D_{PS}\tau_T)^{1/2}$ = 25 nm. This distance is less than half of the average diffusion distance of singlet oxygen in water (*ca*. 86 nm), indicating that the "active triplet excited state volume" (defined analogously to the active singlet oxygen volume) is defined by a spherical aqueous shell that is a lot shallower than that of singlet oxygen. In practice, for MB there are only 5 photosensitizer molecules in the aqueous component of the active triplet excited state volume. For DO15 this number is closer to 4 molecules (recall that for DO15 a significant higher number of molecules will be in the membranes, hence further depleting the aqueous bulk).

Therefore, in our actual experimental conditions, while there are *ca.* 150 molecules of singlet oxygen being generated in the active singlet oxygen volume per second for both DO15 and MB, the number for triplet excited states generated in the triplet diffusion shell would be significantly smaller. In other words, it is a lot more probable that singlet oxygen molecules would be able to visit all lipids in few minutes of irradiation, then it is for triplet

excited states. In terms of the triplets that diffuse aqueous component of the active triplet excited state volume, the number that reaches the membranes will be for MB and DO15, respectively, 12.7 s^{-1} ($5*Q_T = 5*2.53$) and 5.4 s^{-1}, ($4*Q_T = 1.36$), *i.e.*, the number of diffusing triplets able to reach the membrane will be twice as large for MB than for DO15. As happens to the number of singlet oxygen molecules able to reach the membrane, triplets coming from the aqueous shell cannot explain the higher efficiency of DO15 to permeabilize and oxidize membranes.

As both kinds of diffusing species cannot explain the higher efficiency of DO15, we advocate that the differences arise from the triplets that are generated in the membranes and that can directly reach the lipid double bonds. For MB, 10 triplets s^{-1} ($4*Q_T = 4*2.53$) will be generated per second, while for DO15 the number raises to 103 triplets s^{-1} ($76*Q_T = 76*1.36$), given its larger distribution in the lipid phase (recall that the model predicts that there are 4 and 76 photosensitizer molecules dissolved in the lipid phase per liposome for MB and DO15, respectively). When the higher overlap of DO15 triplets with the lipid double bound is considered in the calculation (1.3-fold higher for DO15), the efficiency of generation of triplets that have a higher chance encounter a double bond can be calculated as 76*1.3*1.36 = 134, which is 13 times larger than for MB (4*2.53*1 = 10). Consequently, for DO15 in 10 minutes of irradiation there will be four times more possible triplet hits with the double bound (8×10^4) than the number of double bonds per liposome (1.9×10^4); on the other hand, the availability of triplets to oxidize membranes is comparatively limited for MB.

2.4. Singlet Oxygen Generation by MB and DO15 with POPC Bilayers

The figure below shows singlet oxygen luminescence profiles for both photosensitizers in POPC liposomes, at exact the same conditions used for most of our experiments (*e.g.*, the oxidized lipid analyses from Figures 2C and 3D), with the excitation wavelength and lipid and photosensitizer concentrations. Note that the amplitude of the signal is somewhat larger for MB compared with DO15, which is related to the higher absorption cross-section of MB in this excitation wavelength and is in accordance to our calculations of the number of singlet oxygen molecules generated per second (see *2.3*). Even though a detailed kinetics analysis is beyond the scope of this article, we note that the luminescence profiles have different "shapes", translating the different chemical environments of the dyes (*i.e.* part of the DO15 molecules are membrane-bound)[7].

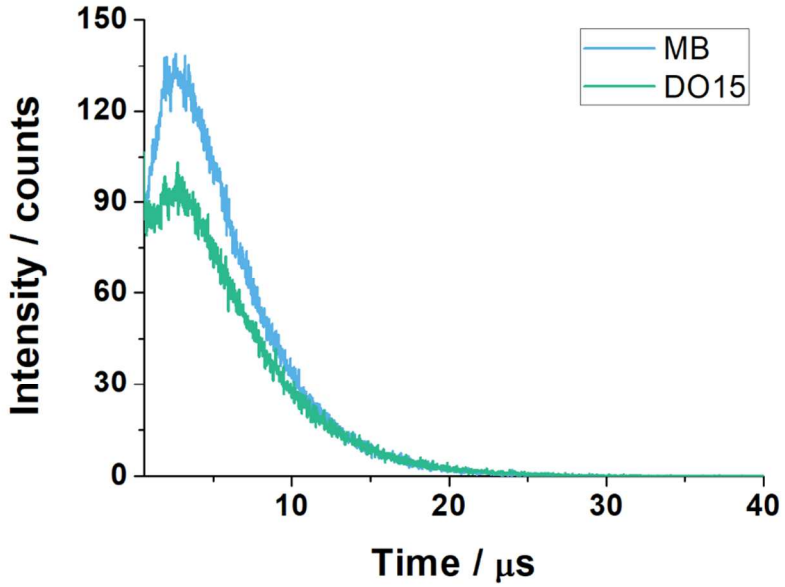

Figure S6. Singlet oxygen luminescence profiles at 1270 nm obtained by exciting MB or DO15 (15 μM) at 631 nm in the presence of POPC liposomes, following the same sample composition as for most of our experiments. The displayed profiles are the average of 9 individual measurements.

2.5. Effect of DO15 and its Bleached Counterpart on Membrane Permeabilization

Bleached DO15 molecules were obtained by incubation of DO15 with NADH and argon, followed by 5 min irradiation, after which liposomes were added to the sample. NADH is able to reduce phenothiazinium triplet excited states, leading to the formation of their leuco derivative, which is not photoactive. This product can be detected if the reaction is performed under low oxygen concentration, because oxygen can re-oxide the leuco form to the visible-light absorbing dye[48]. If compared with pristine DO15, note that the sample that is purged with argon and briefly irradiated has a much-decreased absorption band in the red region, which is partially recovered after 30 min in the dark, due to the effect of oxygen re-entering the cuvette (Figure S7, inset). During the photochemical reactions performed with DO15 and liposomes (Figure 1, main manuscript), there is a clear photobleaching of DO15 due to the electron transfer reaction with the double bond of the lipids, forming the reduced leuco form of the dye. Therefore, we could test whether or not the leuco form of DO15 can interfere with the membrane integrity, causing membrane permeabilization. The percentage of CF released in the different experimental conditions tested in this control experiment is shown in Figure S7. Note that neither DO15 in the dark (NADH + DO15 or "dark" in Figure 1B) nor bleached DO15 molecules (NADH + DO15 + argon) are able to release CF with any measurable difference compared with the control (NADH solution only). Note also that the irradiation of vesicles in the presence of unbleached DO15 (DO15 + light) allows extensive CF released, as also shown in Figure 1 of the main manuscript. Therefore, the leuco form of DO15 does not cause CF release.

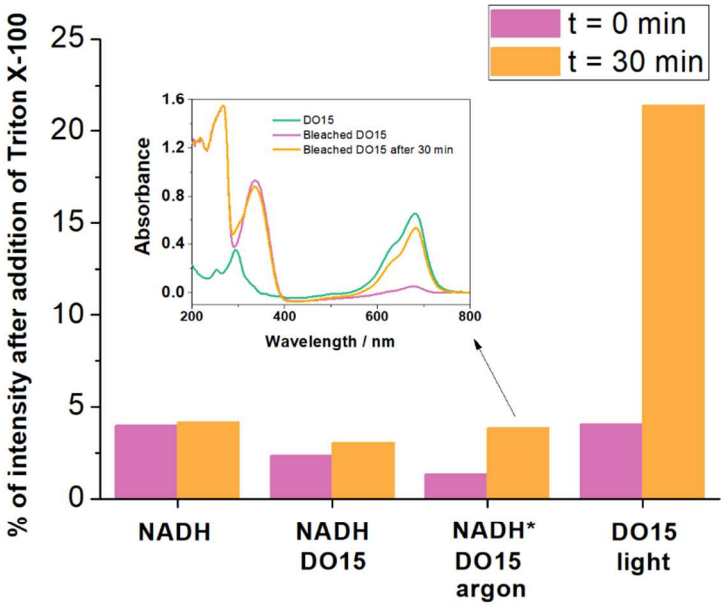

Figure S7. 5(6)-carboxyfluorescein (CF) release from POPC liposomes treated with (i) NADH only; (ii) NADH + DO15; (iii) NADH + DO15 + argon; (iii) DO15 + light (631 nm, 72 ± 1 W m^{-2}). For sample (ii), to which we refer as "bleached DO15", bubbling with argon was followed by *ca.* 5 min irradiation (631 nm, 72 ± 1 W m^{-2}) before liposome addition to the cuvette. Samples were prepared in 10 mM Tris 0.3 M NaCl, pH = 8 with 0.24 mM NADH or 15 μM DO15. Intensities (excitation: 480 nm, emission: 517 nm) are expressed as percentages of the intensity obtained after addition of 0.1% Triton X-100 after the end of the experiment. Inset: absorption spectra for an aqueous sample of DO15 and for a sample of bleached DO15 before and after 30 min in the dark.

2.6. Effect of an Iron Chelator on Membrane Permeabilization

The iron chelator DTPA did not prevent CF leakage, suggesting that radical reactions are initiated by the photosensitizer and not by traces of metal cations in solution (the reduction potential of the pair Fe(III)DTPA/Fe(II)DTPA is 30 mV, compared to 120 mV for Fe(III)EDTA/Fe(II)EDTA[49,50]).

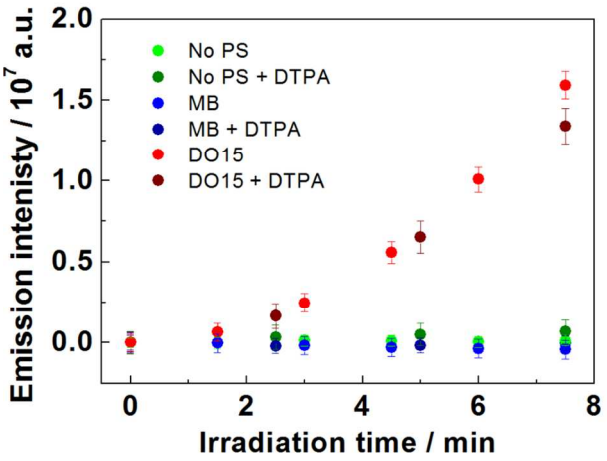

Figure S8. CF emission intensity as a function of irradiation time for POPC liposomes irradiated (631 nm LED with 72 ± 1 W m^{-2} irradiance) in the absence (control) or in the presence of photosensitizers (15 µM MB or DO15) in 10 mM Tris buffer (pH = 8) with 0.3 M sodium chloride. Samples were treated or not with 100 µM DTPA.

2.7. Membrane Permeabilization Kinetics of MB and DO15 in the Presence of Polyunsaturated Lipids

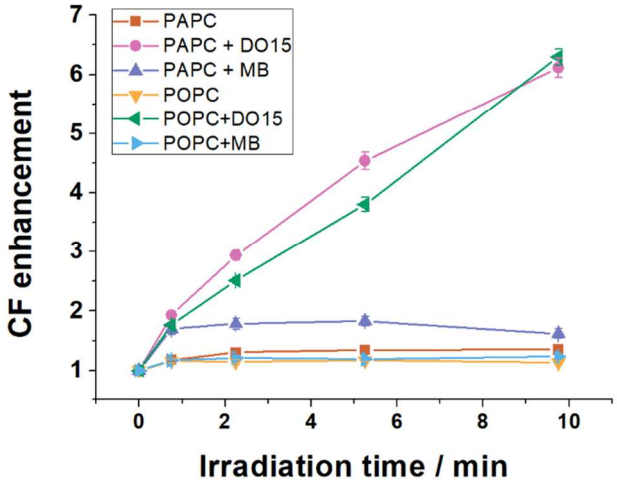

Figure S9. Fluorescence enhancement kinetics of 5(6)-carboxyfluorescein (CF) encapsulated in 1-palmitoyl-2-arachidonoyl-*sn*-glycero-3-phosphocholine (PAPC) or 1-palmitoyl-2-oleoyl-*sn*-glycero-3-phosphocholine (POPC) liposomes irradiated (631 nm, 72 ± 1 W m^{-2}) without PS (controls) or with either MB or DO15 (15 μM) in 10 mM Tris 0.3 M NaCl, pH = 8.

2.8. Quantification of Major Lipid Oxidation Products: Hydroperoxides, Alcohols and Ketones

Figure S10 shows a typical UHPLC-UV chromatogram for POPC liposomes irradiated with DO15. A number of overlapping peaks with retention times shorter than for non-oxidized POPC (not displayed in the presented chromatogram) emerge during irradiation, indicating the formation of oxidized lipid products. These peaks are eluted at similar retention times, absorbing mostly at 190 nm (lipid double bond) or 230 nm (α,β-unsaturated ketones[51] – note that POPC is a monounsaturated lipid and, hence, does not form conjugated dienes that would absorb in this same region).

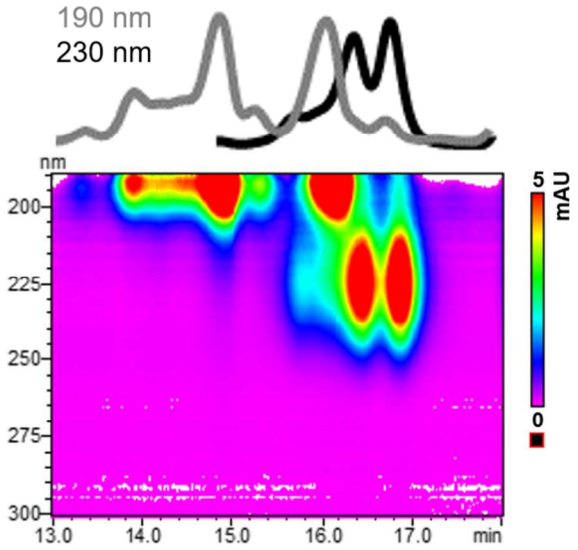

Figure S10. Chromatogram resulting from the UHPLC-UV analysis of POPC liposomes irradiated (631 nm LED with 72 ± 1 W m-2 irradiance) for 15 min in the presence of 15 μM DO15 in 10 mM Tris buffer (pH = 8) with 0.3 M sodium chloride. Detection was in the 180-300 nm range, being additionally presented the extracted chromatograms for 190 and 230 nm (grey and black lines, respectively).

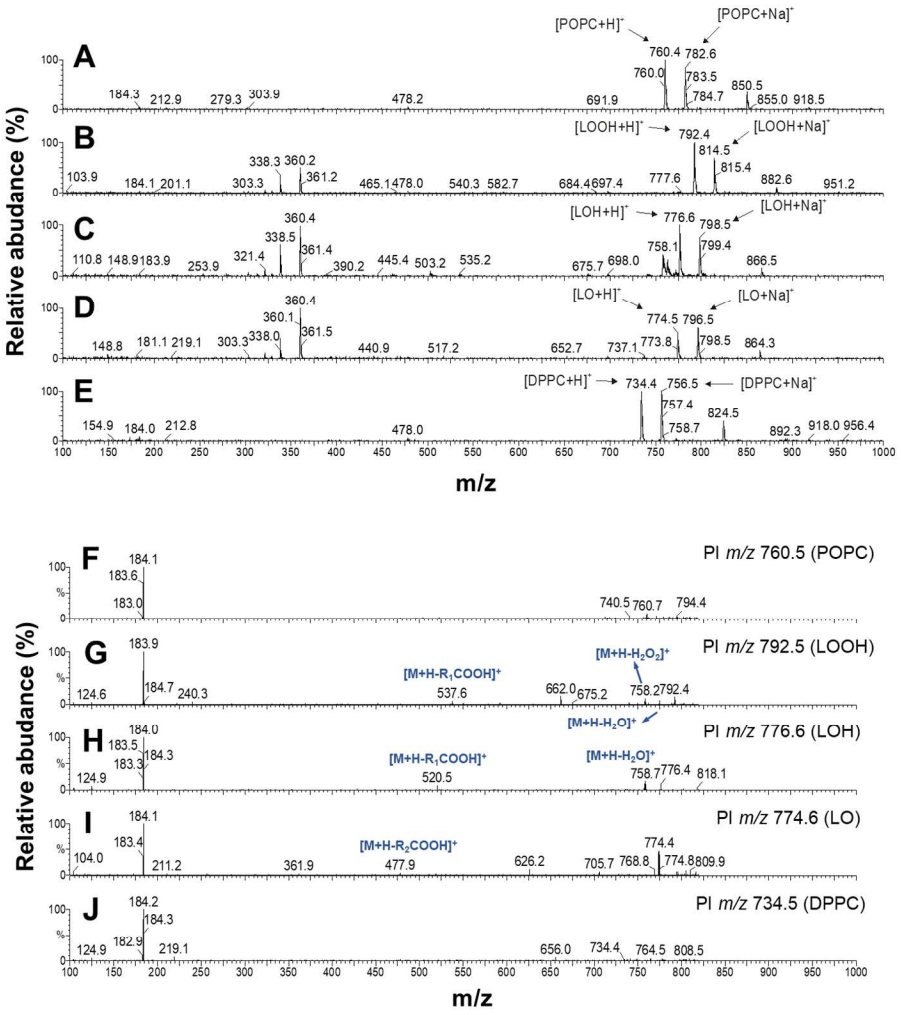

Figure S11. (A) MS1 spectra obtained by HPLC-MS/MS analysis (ESI+) of (A) POPC, (B) POPC hydroperoxides (LOOH), (C) POPC alcohols (LOH), (D) POPC ketones (LO) and (E) DPPC. Product ion (PI) spectra of the $[M+H]^+$ ion for (F) POPC, (G) LOOH, (H) LOH, (I) LO and (J) DPPC. Data were acquired with a Quattro II mass spectrometer, according to *1.8*.

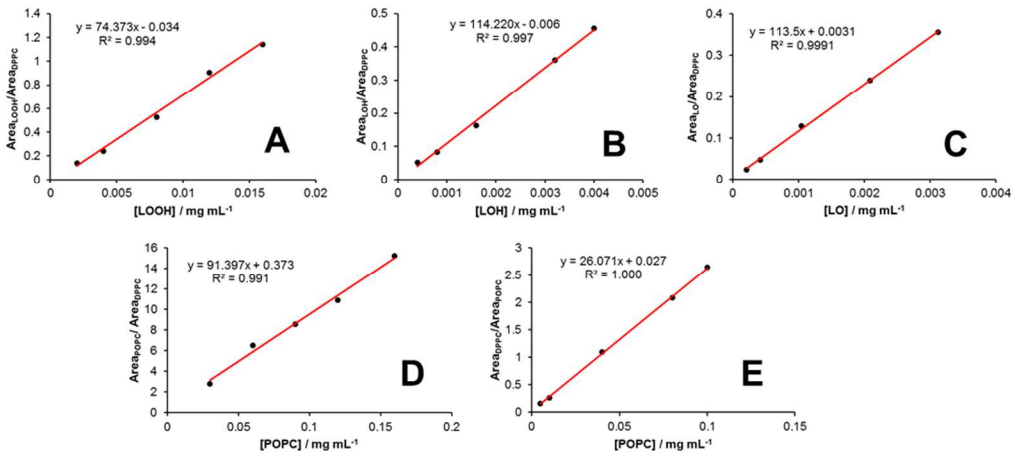

Figure S12. Calibration curves constructed from integration of the peaks from MRM chromatograms for the transitions $[M+H]^+ \rightarrow m/z$ 184 for the synthesized oxidized lipid standards (LOOH: hydroperoxides; LOH: alcohols; LO: ketones) and for POPC and DPPC. For all curves, except (E), DPPC was used as internal standard. In order to test the linearity of DPPC response in the studied concentration range, POPC was used as internal standard instead for (E). All points have signal/noise ratio larger than 6. Data were acquired with a Quattro II mass spectrometer, according to *1.8*.

2.9. Quantification of Lipid Aldehydes

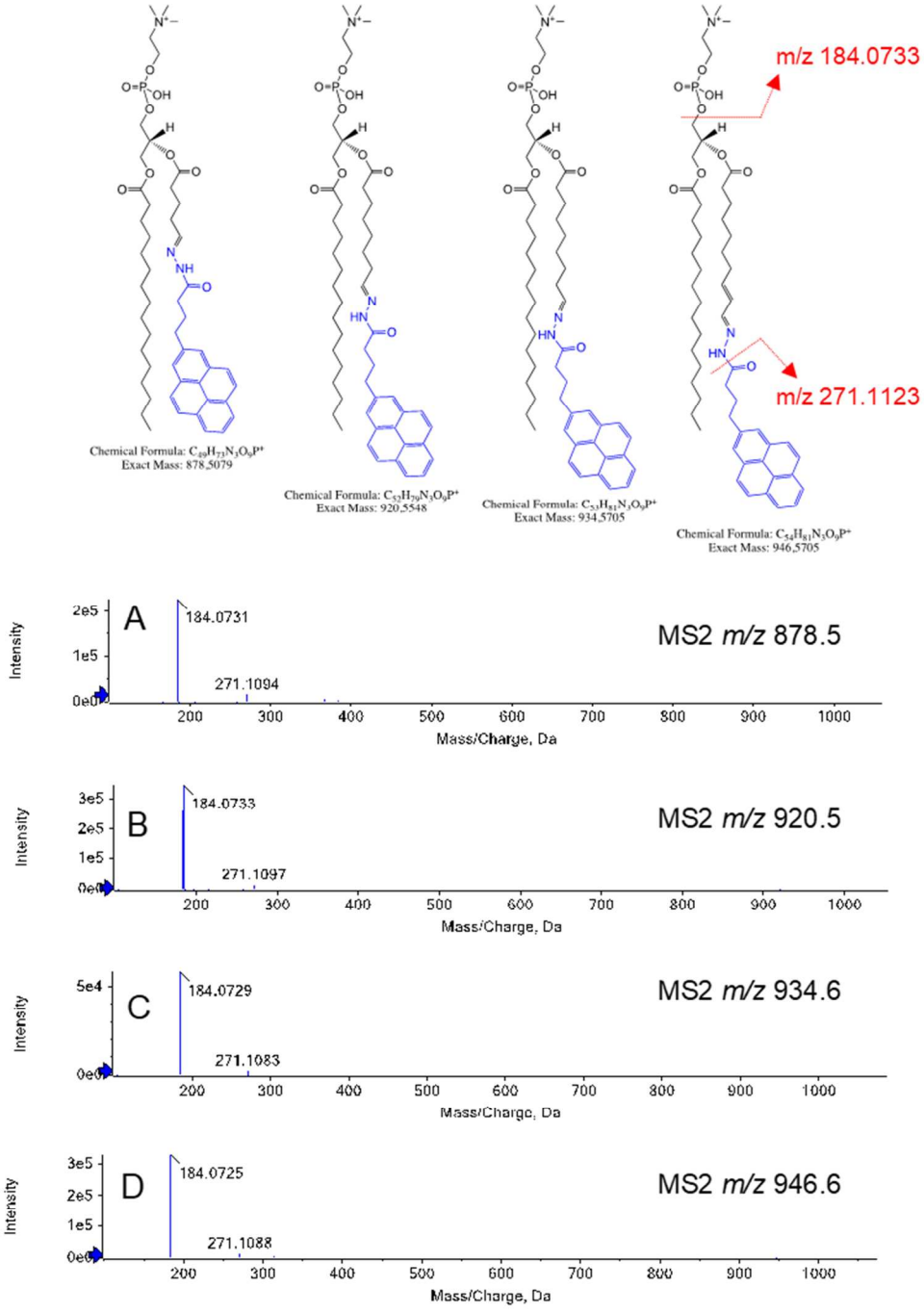

Figure S13. MS2 (ESI+) spectra for the $[M+H]^+$ ions corresponding to the PBH adducts of the internal standard (A: POVPC) and the three analytes (B: ALDOPC-8; C: ALDOPC; D: ALDOPC-10) as determined by UHPLC-MS/MS analysis of a sample irradiated (631 nm LED with 72 ± 1 W m^{-2} irradiance) for 20 min with 15 µM DO15. The structure of the each PBH adduct is represented on the top part of the figure, as well as the two main transitions observed: $[M+H]^+ \rightarrow m/z$ 184.0733, used for quantification, and $[M+H]^+ \rightarrow m/z$ 271.1123, used for identity confirmation. Data were acquired with a Triple TOF 6600 mass spectrometer, according to *1.10*.

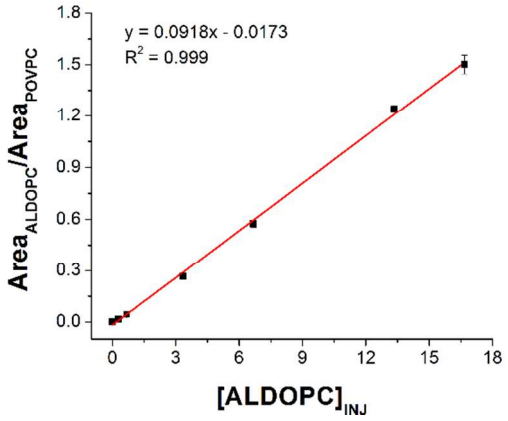

Figure S14. Calibration curve obtained by integration of the parallel reaction monitoring (PRM) chromatogram peaks corresponding to the $[M+H]^+ \rightarrow m/z$ 184.0733 transitions of PBH adducts of the standard ALDOPC and the internal standard POVPC. Data were acquired with a Triple TOF 6600 mass spectrometer, according to *1.10*.

2.10. Simulation of Oxidized Lipid Membranes

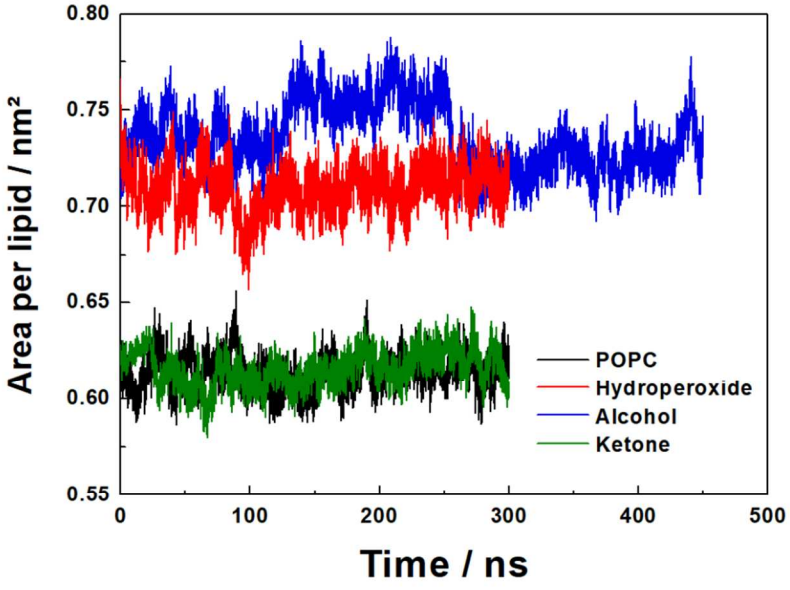

Figure S15. Area per lipid of the simulated systems during 300 ns of simulation. The trajectory for the POPC alcohols was extended until convergence.

Table S4. Properties of simulated single-component membranes composed of POPC and its oxidation products.

Membrane system	Area per lipid / nm²	Membrane thickness / nm	Distance between P-C9 / nm
POPC	0.620(5)	3.78(3)	1.10(3)
LOOH	0.712(2)	3.30(1)	0.88(2)
LOH	0.74(2)	3.17(1)	0.83(7)
LO	0.621(3)	3.83(9)	1.25(4)
ALDOPC	-	2.77(1)	0.43(6)

* LOOH: hydroperoxide; LOH: alcohol; LO: ketone. The numbers between brackets represent the uncertainties in the last digits. Uncertainties were estimated by dividing each trajectory in two parts and calculating the standard deviation of the property values recorded in each part.

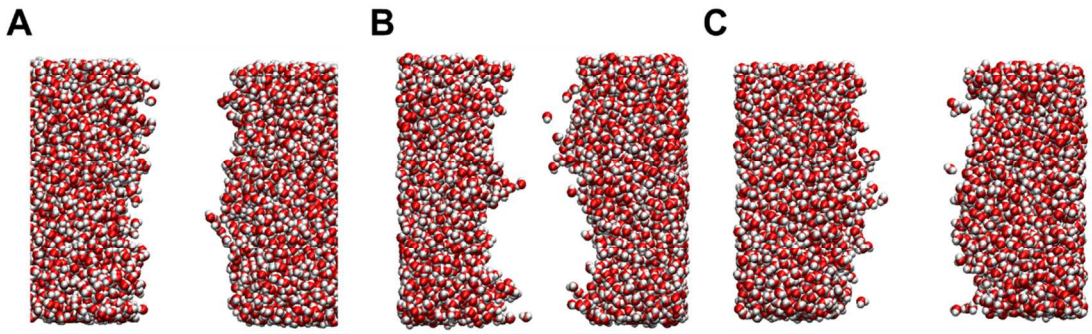

Figure S16. Snapshots from molecular dynamics simulations of oxidized lipid membranes, showing only water molecules (lipids omitted, analogously to Figure 4E in the main text). Single-component membranes were composed by POPC-derived (A) hydroperoxides, (B) alcohols and (C) ketones.

2.11. Spectral Changes of Photosensitizers/Lipids During Irradiation

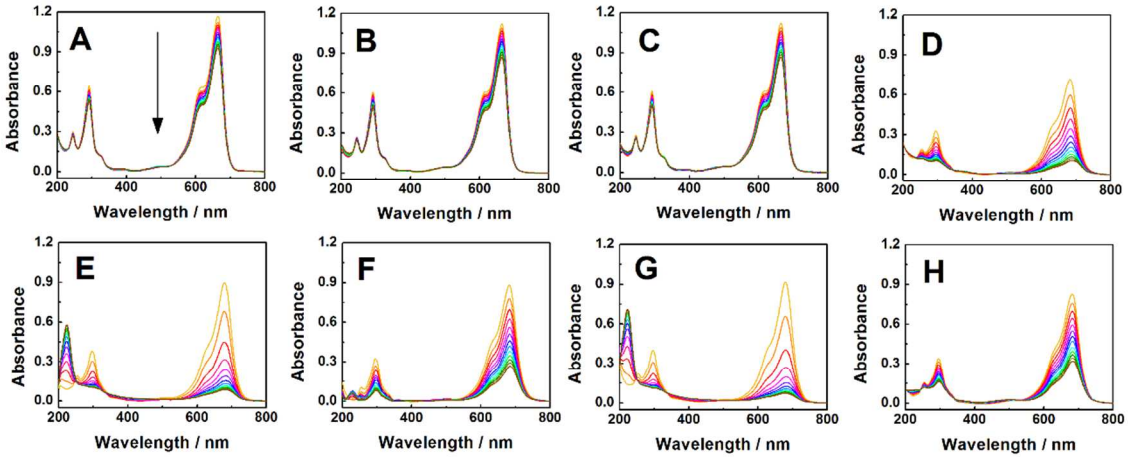

Figure S17. Absorption spectra of 15 µM photosensitizer aqueous samples irradiated with a 650 nm diode laser (35 mW) in 10 min (F) or 5 min time-steps (all others). The yellow curve corresponds to t = 0. MB was employed for graphs A-C, which contained (A) no liposomes, (B) POPC liposomes and (C) POPC hydroperoxide liposomes. DO15 was employed for figures D-H, which contained (D) no liposomes, (E) POPC liposomes, (F) POPC hydroperoxides liposomes, (G) DOPC liposomes and (H) DPPC liposomes. Graphs B, C and F-H were corrected for scattering.

2.12. Effect of Double Bond Concentration on the Photobleaching Rate of DO15

Even though photobleaching rates of DO15 are mainly dependent on the direct reaction with the lipid double bond, similar rates were measured in POPC and DOPC (Figure 5C, main text). The figure below shows that in two-component membranes containing smaller percentages of unsaturated chains, different rates are measured depending on double bond concentration (*ca.* 0.045 min^{-1} for DMPC:POPC 8:2 and DMPC:DOPC 9:1 *versus ca.* 0.034 min^{-1} for DMPC:POPC 9:1). By assuming that the background photobleaching in DMPC is independent from the double-bond dependent photobleaching, we can subtract the rate of photobleaching in DMPC (*ca.* 0.015 min^{-1}) from the rate constants for the two-components membranes. Note that the rate of DMPC:DOPC 9:1 and DMPC:POPC 8:2 (*ca.* 0.030 min^{-1}) is significantly larger than that of DMPC:POPC 9:1 (*ca.* 0.020 min^{-1}), with the latter being ca. 65% of the former. We understand that other factors (namely the biophysical properties of membranes and the interaction of the DO15 with different lipid species) most probably account for the deviation from the expected value (50%, *i.e.*, the rate for DMPC:POPC 9:1 being half of the others). Nonetheless, it is evident that the rate of photobleaching is dependent on the concentration of double bonds present in the membrane, suggesting that in pure POPC there are already enough double bonds diffusing in the membrane, so that no difference is observed when their concentrations are doubled (as is pure DOPC).

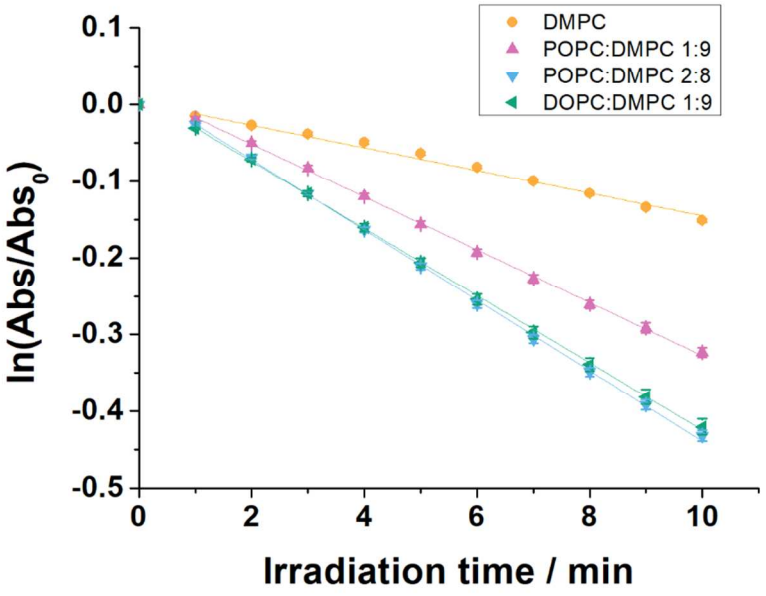

Figure S18. Photobleaching curves for DO15 in the presence of liposomes containing different percent concentrations of double bonds. Samples containing 15 μM DO15 were irradiated (631 nm, 72 ± 1 W m^{-2}) for 1 h and the absorbance at 680 nm was measured every 1 min. Liposomes compositions (mol/mol) were: (i) DMPC; (ii) DMPC:POPC 9:1; (iii) DMPC:POPC 8:2; (iv) DMPC:DOPC 9:1.

2.13. Activation of the Fluorogenic Probe H_2B-PMHC

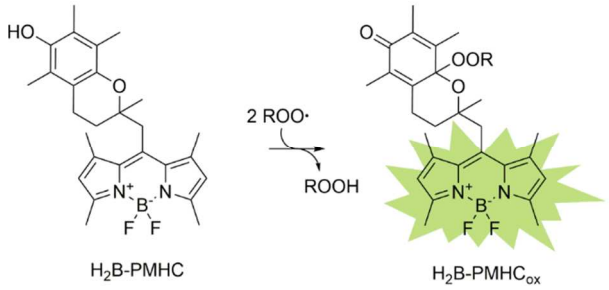

Figure S19. Emission enhancement of the fluorogenic probe H_2B-PMHC occurs upon reaction with peroxyl ($ROO^{\bullet}$) or alkoxyl radicals[2].

2.14. Effect of pH on Giant Unilamellar Vesicles Impermeability to Sugars: Hock Cleavage

GUVs made of POPC and POPC hydroperoxides were shown to be stable from pH 3.5 to 8.8 (Figure S20A-B). In this pH range, both POPC and POPC hydroperoxide GUVs preserved their refraction index contrast (*i.e.* did not get permeabilized towards sugars – see [8] for application of phase contrast microscopy to detected changes in GUV permeability), with less than 2% of GUVs showing permeabilization and no pH-dependent trend being observed. Of note, the population of GUVs made of pristine POPC was significantly reduced at pH 2.6 (less than 10 GUVs per field being observed, with *ca.* 13% of permeabilized vesicles), for which reason our studies were only carried out above this pH. In addition to that, we tested if the same findings held true for PAPC and its hydroperoxides. We were unable to grow GUVs with 100% PAPC hydroperoxides, for which reason we resorted to membranes containing PAPC:PAPC hydroperoxides 1:1 (w/w). In general, we observed that vesicles made of both PAPC and PAPC hydroperoxides are a bit more unstable than those made of POPC, resulting in *ca.* 10-fold less vesicles per observation field. As can be seen in Figure S20C, PAPC hydroperoxides vesicles are stable at pH close to neutral. This already suggests that, even if Hock cleavage occurs, it is not meaningful for any of the studied membrane compositions (*i.e.*, POPC and PAPC) at the pH conditions used in here, which are also present in most biological membranes. In addition, by lowering the pH we did not detect a consistent trend of increased membrane permeabilization as pH is decreased (Figure S20D), with the percentage of permeabilized GUVs being comparable to pristine PAPC. We also note that the Lewis-acid Fe(III) did not promote membrane permeabilization, with both POPC hydroperoxides and PAPC hydroperoxides GUVs retaining contrast (Figure S20E).

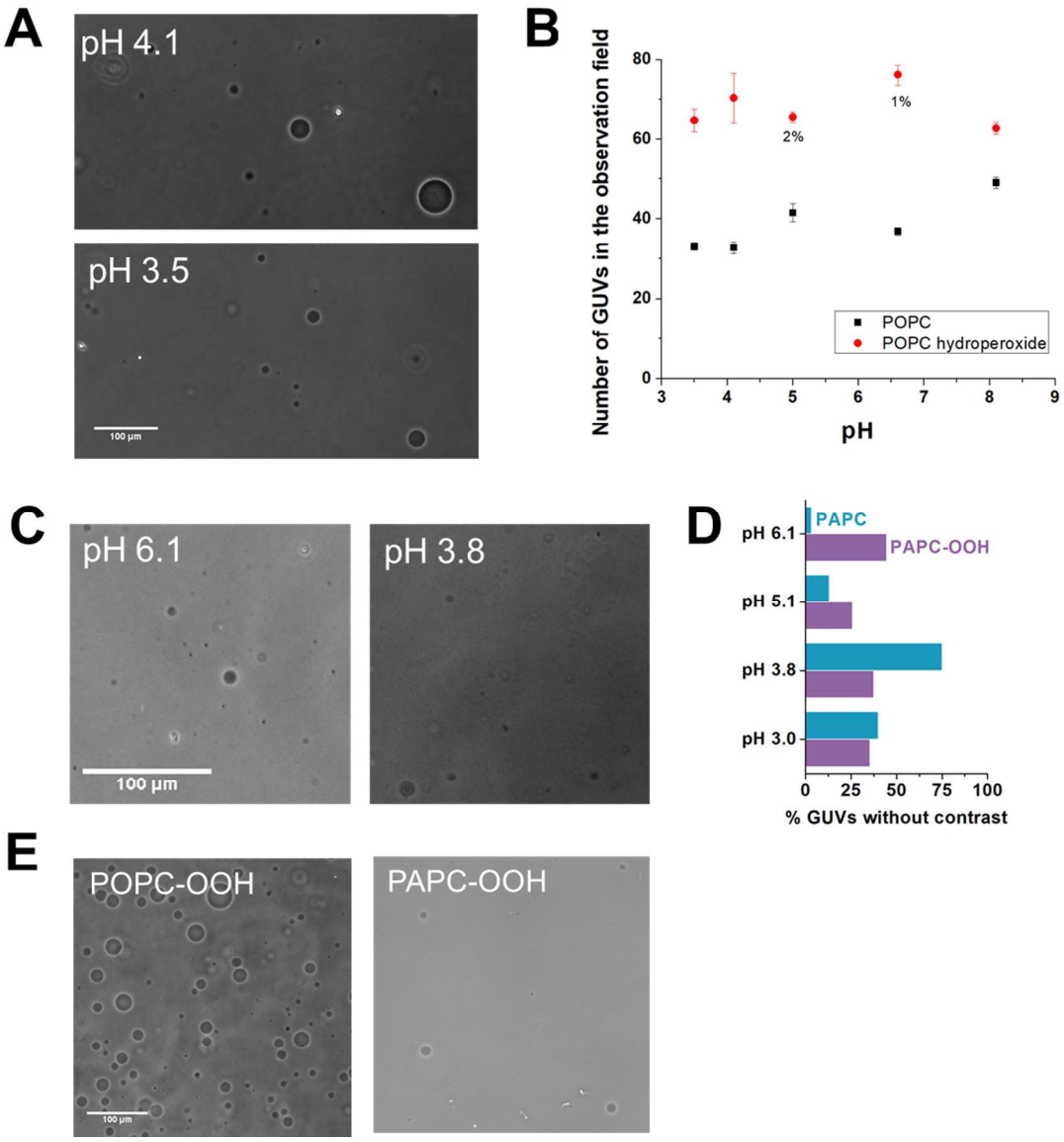

Figure S20. (A) Phase contrast microscopy images of POPC hydroperoxides GUVs at pH 4.1 and 3.5. (B) Average number of GUVs in the observation field as a function of pH, for POPC and POPC hydroperoxides GUVs. In the sole cases where GUVs without contrast were observed, their percentage contribution to the total GUV population is also provided. (C) Phase contrast microscopy images of GUVs containing PAPC:PAPC hydroperoxides 1:1 (mol/mol) after 1 h of observation at pH 6.1 and 3.8. (D) Percentage of GUVs without contrast as a function of pH for pure PAPC GUVs and for GUVs containing PAPC:PAPC hydroperoxides 1:1 (mol/mol) (PAPC-OOH), after 1 h of observation. (E) Phase contrast microscopy images of POPC hydroperoxides GUVs (POPC-OOH) and of GUVs containing PAPC:PAPC hydroperoxides 1:1 (mol/mol) (PAPC-OOH) in the presence of 31 µM Fe(III).

In order to test our ability to detect membrane permeabilization in such experiments, we performed a control experiment in which we added 31 μM of Fe(II) to the GUVs (note that the Fe(II) concentration is orders of magnitude smaller than that of added H^+ for the pH-dependence measurements). Note that POPC hydroperoxides (Figure S21A) and PAPC hydroperoxides (Figure S21B) all GUVs partially or completely lost contrast (*i.e.*, suffered permeabilization) with the increase of time in contact with the Fe(II) solution, showing that the experimental system responds positively for oxidative damage in the membrane. For some GUVs, complete bursting was also observed. These results are consistent with the effect Fe(II) catalyzing, by Fenton reaction, the formation of hydroxyl radical and inducing radical chain reactions. Together, these results endorse both the chemical and biophysical stability of hydroperoxides membranes and the need for radical-mediated pathways for membrane permeabilization.

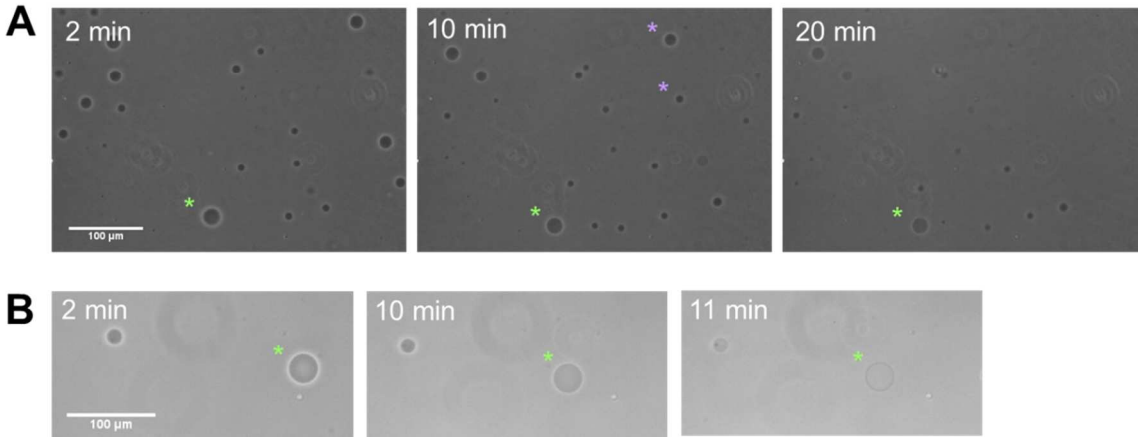

Figure S21. (A) Phase contrast microscopy images of POPC hydroperoxides GUVs after 2, 10 and 20 min of exposure to 31 μM Fe(II). (B) Phase contrast microscopy images of GUVs containing PAPC:PAPC hydroperoxides 1:1 (mol/mol) after 2, 10 and 11 min of exposure to 31 μM Fe(II). Green stars exemplify GUVs that lost contrast partially in (A) or totally in (B). Purple stars sign GUVs that burst in the succeeding frame.

2.15. Comparison of Expected Products: Hock Cleavage versus *Alkoxyl Radical β–scission*

Although being both putative sources of phospholipid aldehydes, Hock cleavage and alkoxyl radical β-scission require different precursor species and can lead to different products. The former mechanism applies to allylic hydroperoxides, whose double bond is lost when a last reaction intermediate suffers cleavage after a nucleophilic attack by water[52]. Note in Scheme 3 (main text) that in practical terms, the precursor is split in two parts in the position where the bond connecting the carbon bearing the -OOH group and the unsaturated carbon originally was. As a result, only saturated aldehyde products are formed from a monounsaturated precursor. On the other hand, alkoxyl radical β-scission is based on the cleavage of the bond connecting the carbon bearing the -O$^{\bullet}$ group and any of the adjacent carbons, meaning that for each alkoxyl radical there exist two cleavage possibilities. As for the cleavage possibilities leading to phospholipid aldehydes, if the unsaturation is located between the carbon holding the -O$^{\bullet}$ and the lipid headgroup, the product of the alkoxyl radical β-scission is an unsaturated phospholipid aldehyde. On the other hand, if the unsaturation is located between the carbon holding the -O$^{\bullet}$ and the terminal methyl group, the product will be a saturated aldehyde phospholipid. Therefore, if the chain breaking mechanism is alkoxyl radical β-scission we would observe both saturated and unsaturated truncated aldehyde phospholipids, which was the case indeed. This concept is illustrated in the figure below, in which we compare the outcomes of Hock cleavage and alkoxyl radical β-scission for the isomers 9-OOH and 10-OOH of POPC hydroperoxides formed by the ene-reaction. We also detected the aldehyde originated from

the alkoxyl radical substituted in the C8, which is known to be formed in radical-mediated oxidation of oleic acid[53].

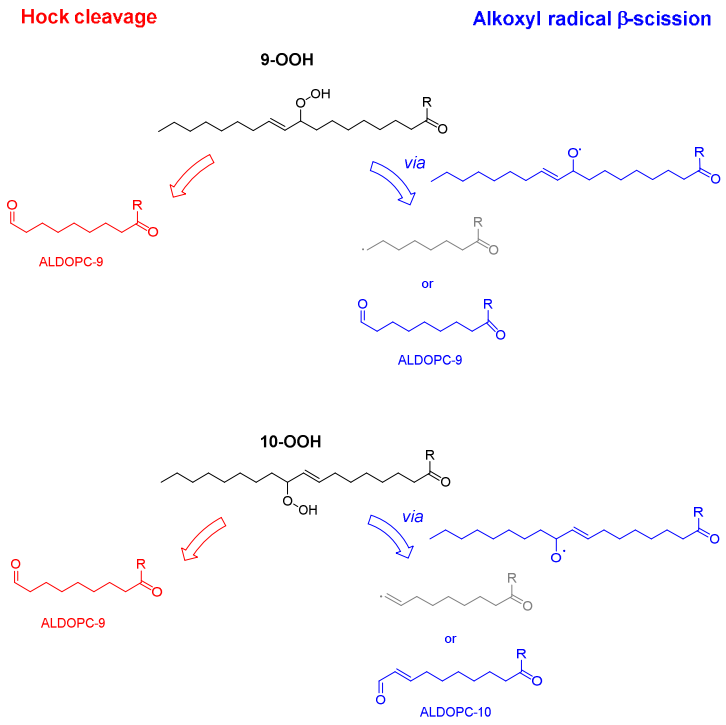

Figure S22. Expected phospholipid products formed by Hock cleavage and alkoxyl radical β-scission from POPC hydroperoxide isomers 9-OOH and 10-OOH.

3. References

(1) Wainwright, M.; Meegan, K.; Loughran, C. Phenothiazinium Photosensitisers IX. Tetra- and Pentacyclic Derivatives as Photoantimicrobial Agents. *Dye. Pigment.* **2011**, *91* (1), 1–5.

(2) Krumova, K.; Friedland, S.; Cosa, G. How Lipid Unsaturation, Peroxyl Radical Partitioning, and Chromanol Lipophilic Tail Affect the Antioxidant Activity of α-Tocopherol: Direct Visualization via High-Throughput Fluorescence Studies Conducted with Fluorogenic α-Tocopherol Analogues. *J. Am. Chem. Soc.* **2012**, *134* (24), 10102–10113.

(3) Aschi, M.; D'Archivio, A. A.; Fontana, A.; Formiglio, A. Physicochemical Properties of Fluorescent Probes: Experimental and Computational Determination of the Overlapping p K a Values of Carboxyfluorescein. *J. Org. Chem.* **2008**, *73* (9), 3411–3417.

(4) Chen, R. F.; Knutson, J. R. Mechanism of Fluorescence Concentration Quenching of Carboxyfluorescein in Liposomes: Energy Transfer to Nonfluorescent Dimers. *Anal. Biochem.* **1988**, *172* (1), 61–77.

(5) Weinstein, J.; Yoshikami, S.; Henkart, P.; Blumenthal, R.; Hagins, W. Liposome-Cell Interaction: Transfer and Intracellular Release of a Trapped Fluorescent Marker. *Science* **1977**, *195* (4277), 489–492.

(6) Engelmann, F. M.; Mayer, I.; Gabrielli, D. S.; Toma, H. E.; Kowaltowski, A. J.; Araki, K.; Baptista, M. S. Interaction of Cationic Meso-Porphyrins with Liposomes, Mitochondria and Erythrocytes. *J. Bioenerg. Biomembr.* **2007**, *39* (2), 175–185.

(7) Bacellar, I. O. L.; Pavani, C.; Sales, E. M.; Itri, R.; Wainwright, M.; Baptista, M. S. Membrane Damage Efficiency of Phenothiazinium Photosensitizers. *Photochem. Photobiol.* **2014**, *90* (4), 801–813.

(8) Mertins, O.; Bacellar, I. O. L.; Thalmann, F.; Marques, C. M.; Baptista, M. S.; Itri, R. Physical Damage on Giant Vesicles Membrane as a Result of Methylene Blue Photoirradiation. *Biophys. J.* **2014**, *106* (1), 162–171.

(9) Pavani, C.; Uchoa, A. F.; Oliveira, C. S.; Iamamoto, Y.; Baptista, M. S. Effect of Zinc Insertion and Hydrophobicity on the Membrane Interactions and PDT Activity of Porphyrin Photosensitizers. *Photochem. Photobiol. Sci.* **2009**, *8* (2), 233–240.

(10) Stewart, J. C. Colorimetric Determination of Phospholipids with Ammonium Ferrothiocyanate. *Anal. Biochem.* **1980**, *104* (1), 10–14.

(11) Bligh, E. G.; Dyer, W. J. A Rapid Method of Total Lipid Extraction and Purification. *Can. J. Biochem. Physiol.* **1959**, *37* (8), 911–917.

(12) Pulfer, M.; Murphy, R. C. Electrospray Mass Spectrometry of Phospholipids. *Mass Spectrom. Rev.* **2003**, *22* (5), 332–364.

(13) Han, X.; Gross, R. W. Structural Determination of Picomole Amounts of Phospholipids via Electrospray Ionization Tandem Mass Spectrometry. *J. Am. Soc.*

Mass Spectrom. **1995**, *6* (12), 1202–1210.

(14) Mansano, F. V.; Kazaoka, R. M. A.; Ronsein, G. E.; Prado, F. M.; Genaro-Mattos, T. C.; Uemi, M.; Di Mascio, P.; Miyamoto, S. Highly Sensitive Fluorescent Method for the Detection of Cholesterol Aldehydes Formed by Ozone and Singlet Molecular Oxygen. *Anal. Chem.* **2010**, *82* (16), 6775–6781.

(15) Miyamoto, S. Hidroperóxidos de Lipídios Como Fonte Biológica de Oxigênio Singlete: Estudos Com Marcação Isotópica, Espectrometria de Massas e Luminescência, Universidade de São Paulo: São Paulo, 2005.

(16) Miyamoto, S.; Martinez, G. R.; Rettori, D.; Augusto, O.; Medeiros, M. H. G.; Di Mascio, P. Linoleic Acid Hydroperoxide Reacts with Hypochlorous Acid, Generating Peroxyl Radical Intermediates and Singlet Molecular Oxygen. *Proc. Natl. Acad. Sci.* **2006**, *103* (2), 293–298.

(17) Terao, J.; Shibata, S. S.; Matsushita, S. Selective Quantification of Arachidonic Acid Hydroperoxides and Their Hydroxy Derivatives in Reverse-Phase High Performance Liquid Chromatography. *Anal. Biochem.* **1988**, *169* (2), 415–423.

(18) Derogis, P. B. M. C. Estudos Dos Produtos Da Oxidação Não Enzimática Do Ácido Docosahexaenoico Como Possíveis Biomarcadores Para Doenças Neurodegenerativas, Universidade de São Paulo: São Paulo, 2014.

(19) Dong, J.; Chen, W.; Wang, S.; Zhang, J.; Li, H.; Guo, H.; Man, Y.; Chen, B. Jones Oxidation and High Performance Liquid Chromatographic Analysis of Cholesterol in Biological Samples. *J. Chromatogr. B. Analyt. Technol. Biomed. Life Sci.* **2007**, *858* (1–2), 239–246.

(20) Harris, D. C. *Quantitative Chemical Analysis*, 2nd ed.; W.H.Freeman & Co Ltd: New York, 1987.

(21) Buege, J. A.; Aust, S. D. Microsomal Lipid Peroxidation. *Methods Enzymol.* **1978**, *52*, 302–310.

(22) Marsh, D. *Handbook of Lipid Bilayers, Second Edition*; 2013.

(23) Angelova, M. I.; Dimitrov, D. S. Liposome Electroformation. *Faraday Discuss. Chem. Soc.* **1986**, *81*, 303.

(24) Hess, B.; Kutzner, C.; van der Spoel, D.; Lindahl, E. GROMACS 4: Algorithms for Highly Efficient, Load-Balanced, and Scalable Molecular Simulation. *J. Chem. Theory Comput.* **2008**, *4* (3), 435–447.

(25) Van Der Spoel, D.; Lindahl, E.; Hess, B.; Groenhof, G.; Mark, A. E.; Berendsen, H. J. C. GROMACS: Fast, Flexible, and Free. *J. Comput. Chem.* **2005**, *26* (16), 1701–1718.

(26) Kukol, A. Lipid Models for United-Atom Molecular Dynamics Simulations of Proteins. *J. Chem. Theory Comput.* **2009**, *5* (3), 615–626.

(27) Oostenbrink, C.; Villa, A.; Mark, A. E.; van Gunsteren, W. F. A Biomolecular Force Field Based on the Free Enthalpy of Hydration and Solvation: The GROMOS Force-

Field Parameter Sets 53A5 and 53A6. *J. Comput. Chem.* **2004**, *25* (13), 1656–1676.

(28) Berendsen, H. J. C.; Postma, J. P. M.; van Gunsteren, W. F.; Hermans, J. Interaction Models for Water in Relation to Protein Hydration. In *Intermolecular Forces*; Springer Netherlands: Amsterdam, 1981; pp 331–342.

(29) Fischer, J.; Lago, S. Thermodynamic Perturbation Theory for Molecular Liquid Mixtures. *J. Chem. Phys.* **1983**, *78* (9), 5750–5758.

(30) Frisch, M. J. et al. Gaussian 09, Revision D.01. *Gaussian 09, Revision D.01*. 2009.

(31) Cordeiro, R. M.; Miotto, R.; Baptista, M. S. Photodynamic Efficiency of Cationic Meso-Porphyrins at Lipid Bilayers: Insights from Molecular Dynamics Simulations. *J. Phys. Chem. B* **2012**, *116* (50), 14618–14627.

(32) Neto, A. J. P.; Cordeiro, R. M. Molecular Simulations of the Effects of Phospholipid and Cholesterol Peroxidation on Lipid Membrane Properties. *Biochim. Biophys. Acta - Biomembr.* **2016**, *1858* (9), 2191–2198.

(33) Poger, D.; Mark, A. E. On the Validation of Molecular Dynamics Simulations of Saturated and Cis -Monounsaturated Phosphatidylcholine Lipid Bilayers: A Comparison with Experiment. *J. Chem. Theory Comput.* **2010**, *6* (1), 325–336.

(34) Petrov, D.; Margreitter, C.; Grandits, M.; Oostenbrink, C.; Zagrovic, B. A Systematic Framework for Molecular Dynamics Simulations of Protein Post-Translational Modifications. *PLoS Comput. Biol.* **2013**, *9* (7), e1003154.

(35) Durig, J. R.; Little, T. S. Conformational Barriers to Internal Rotation and Vibrational Assignment of Methyl Vinyl Ketone. *J. Chem. Phys.* **1981**, *75* (8), 3660–3668.

(36) Schaich, K. M. Lipid Oxidation: Theoretical Aspects. In *Bailey's Industrial Oil and Fat Products*; John Wiley & Sons, Inc.: Hoboken, NJ, USA, 2005.

(37) Ehrenberg, B.; Gross, E. The Effect of Liposomes' Membrane Composition on the Binding of the Photosensitizers Hpd and Photofrin II. *Photochem. Photobiol.* **1988**, *48* (4), 461–466.

(38) Braslavsky, S. E. Glossary of Terms Used in Photochemistry. *Pure and Applied Chemistry*. 2007, pp 293–465.

(39) Busch, N. A.; Yarmush, M. L.; Toner, M. A Theoretical Formalism for Aggregation of Peroxidized Lipids and Plasma Membrane Stability During Photolysis. *Biophys. J.* **1998**, *75* (6), 2956–2970.

(40) Hackbarth, S.; Bornhütter, T.; Röder, B. Chapter 26. Singlet Oxygen in Heterogeneous Systems. In *Singlet Oxygen : Applications in Biosciences and Nanosciences*; RSC, 2016; pp 27–42.

(41) Weber, G.; Charitat, T.; Baptista, M. S.; Uchoa, A. F.; Pavani, C.; Junqueira, H. C.; Guo, Y.; Baulin, V. A.; Itri, R.; Marques, C. M.; Schroder, A. P. Lipid Oxidation Induces Structural Changes in Biomimetic Membranes. *Soft Matter* **2014**, *10* (24), 4241–4247.

(42) Hackbarth, S.; Röder, B. Singlet Oxygen Luminescence Kinetics in a Heterogeneous Environment – Identification of the Photosensitizer Localization in Small Unilamellar Vesicles. *Photochem. Photobiol. Sci.* **2015**, *14* (2), 329–334.

(43) Tanielian, C.; Wolff, C. Determination of the Parameters Controlling Singlet Oxygen Production via Oxygen and Heavy-Atom Enhancement of Triplet Yields. *J. Phys. Chem.* **1995**, *99* (24), 9831–9837.

(44) Miložič, N.; Lubej, M.; Novak, U.; Žnidaršič-Plazl, P.; Plazl, I. Evaluation of Diffusion Coefficient Determination Using a Microfluidic Device. *Chem. Biochem. Eng. Q. J.* **2014**, *28* (2), 215–223.

(45) Robinson, C. The Diffusion Coefficients of Dye Solutions and Their Interpretation. *Proc. R. Soc. A Math. Phys. Eng. Sci.* **1935**, *148* (865), 681–695.

(46) Kapusta, P. Absolute Diffusion Coefficients: Compilation of Reference Data for FCS Calibration. Picoquant GmbH 2010.

(47) Junqueira, H. C.; Severino, D.; Dias, L. G.; Gugliotti, M. S.; Baptista, M. S. Modulation of Methylene Blue Photochemical Properties Based on Adsorption at Aqueous Micelle Interfaces. *Phys. Chem. Chem. Phys.* **2002**, *4* (11), 2320–2328.

(48) Gabrielli, D.; Belisle, E.; Severino, D.; Kowaltowski, A. J.; Baptista, M. S. Binding, Aggregation and Photochemical Properties of Methylene Blue in Mitochondrial Suspensions. *Photochem. Photobiol.* **2004**, *79* (3), 227–232.

(49) Buettner, G. R. The Pecking Order of Free Radicals and Antioxidants: Liperoxidation, a-Tocopherol, Ascorbate. *Arch. Biochem. Biophys.* **1993**, *300* (2), 535–543.

(50) Asaumi, A.; Ogino, T.; Akiyama, T.; Kawabata, T.; Okada, S. Oxidative Damages by Iron-Chelate Complexes Depend on the Interaction with the Target Molecules. *IUBMB Life* **1996**, *39* (1), 77–86.

(51) Woodward, R. B. Structure and the Absorption Spectra of α,β-Unsaturated Ketones. *J. Am. Chem. Soc.* **1941**, *63* (4), 1123–1126.

(52) Hock Rearrangement. In *Comprehensive Organic Name Reactions and Reagents*; John Wiley & Sons, Inc.: Hoboken, NJ, USA, 2010.

(53) Frankel, E. N. Chemistry of Free Radical and Singlet Oxidation of Lipids. *Prog. Lipid Res.* **1984**, *23* (4), 197–221.